

1 **Diagnostic and model dependent uncertainty of**
2 **simulated Tibetan permafrost area**

3

4 **Wenli Wang¹, Annette Rinke^{1,2}, John C. Moore¹, Xuefeng Cui^{1*}, Duoying Ji¹,**
5 **Qian Li³, Ningning Zhang³, Chenghai Wang⁴, Shiqiang Zhang⁵, David M.**
6 **Lawrence⁶, A. David McGuire⁷, Wenxin Zhang⁸, Christine Delire⁹, Charles**
7 **Koven¹⁰, Kazuyuki Saito¹¹, Andrew MacDougall¹², Eleanor Burke¹³,**
8 **Bertrand Decharme⁹**

9 [1]{State Key Laboratory of Earth Surface Processes and Resource Ecology, College of
10 Global Change and Earth System Science, Beijing Normal University, Beijing 100875,
11 China}

12 [2]{Alfred Wegener Institute Helmholtz Centre for Polar and Marine Research,
13 Potsdam, Germany}

14 [3]{Institute of Atmospheric Physics, Chinese Academy of Sciences, Beijing, China}

15 [4]{School of Atmospheric Sciences, Lanzhou University, Lanzhou, China}

16 [5]{College of Urban and Environmental Sciences, Northwest University, Xi' an,
17 China}

18 [6]{NCAR, Boulder, USA}

19 [7]{U.S. Geological Survey, Alaska Cooperative Fish and Wildlife Research Unit,
20 University of Alaska, Fairbanks, USA}

21 [8]{Department of Physical Geography and Ecosystem Science, Lund University, Lund,
22 Sweden}

23 [9]{GAME, Unit é mixte de recherche CNRS/Meteo-France, Toulouse cedex, France}

24 [10]{Lawrence Berkeley National Laboratory, Berkeley, CA, USA}

1 [11] {Department of Integrated Climate Change Projection Research, Japan Agency for
2 Marine-Earth Science and Technology, Yokohama, Kanagawa, Japan}

3 [12]{School of Earth and Ocean Sciences, University of Victoria, Victoria, BC,
4 Canada}

5 [13]{Met Office Hadley Centre, Exeter, UK}

6 Correspondence to: Xuefeng Cui (xuefeng.cui@bnu.edu.cn)

7

8 **Abstract**

9 We perform a land surface model intercomparison to investigate how the simulation of
10 permafrost area on the Tibetan Plateau (TP) varies among 6 modern stand-alone land
11 surface models (CLM4.5, CoLM, ISBA, JULES, LPJ-GUESS, UVic). We also
12 examine the variability in simulated permafrost area and distribution introduced by 5
13 different methods of diagnosing permafrost (from modeled monthly ground
14 temperature, mean annual ground and air temperatures, air and surface frost indexes).
15 There is good agreement (99 to $135 \times 10^4 \text{ km}^2$) between the two diagnostic methods
16 based on air temperature which are also consistent with the observation-based estimate
17 of actual permafrost area ($101 \times 10^4 \text{ km}^2$). However the uncertainty (1 to $128 \times 10^4 \text{ km}^2$)
18 using the three methods that require simulation of ground temperature is much greater.
19 Moreover simulated permafrost distribution on TP is generally only fair to poor for
20 these three methods (diagnosis of permafrost from monthly, and mean annual ground
21 temperature, and surface frost index), while permafrost distribution using air
22 temperature based methods is generally good. Model evaluation at field sites highlights
23 specific problems in process simulations likely related to soil texture specification,
24 vegetation types and snow cover. Models are particularly poor at simulating permafrost
25 distribution using the definition that soil temperature remains at or below 0°C for 24
26 consecutive months, which requires reliable simulation of both mean annual ground
27 temperatures and seasonal cycle, and hence is relatively demanding. Although models

1 can produce better permafrost maps using mean annual ground temperature and surface
2 frost index, analysis of simulated soil temperature profiles reveals substantial biases.
3 The current generation of land surface models need to reduce biases in simulated soil
4 temperature profiles before reliable contemporary permafrost maps and predictions of
5 changes in permafrost distribution can be made for the Tibetan Plateau.

6

7 **1 Introduction**

8 The Tibetan Plateau (TP) has the highest and largest low-latitude frozen ground in the
9 world, with more than 50% of its area occupied by permafrost (Zhou et al., 2000). The
10 unique geography and plateau climate make the permafrost on TP very different from
11 the Arctic. The TP permafrost is warmer, with only discontinuous and sporadic
12 permafrost (Zhou et al., 2000), has less underground ice (Ran et al., 2012), and has no
13 large forests (Wu, 1980). The active layer thickness ranges from 1 m to 3 m, with some
14 intensely degraded area reaching 4.5 m (Wu and Liu, 2004; Wu and Zhang, 2010;
15 Zhang and Wu, 2012). Freeze/thaw cycles, and the extent of permafrost play an
16 important role in the thermal state of TP. The underlying surface temperature contrast
17 between TP and Indian Ocean is an important controlling factor for both the Asian
18 monsoon and the wider general atmospheric circulation (Xin et al., 2012). As TP gets
19 intensely warmer (IPCC, 2013; Wu et al., 2013), the impact of degraded permafrost on
20 desertification (Li et al., 2014; Yang et al., 2010; Li et al., 2005), water cycling (Cheng
21 and Jin, 2013; Yao et al., 2013), carbon budget (Dörfer et al., 2013; Wang et al., 2008;
22 Schuur et al., 2008;), and infrastructure (Wu and Niu, 2013; Yu et al., 2013) has also
23 become active research topics.

24

25 Hence, the simulation of TP permafrost is motivated both by its global importance and
26 by its unique properties. A number of land surface models (LSMs) (e.g., CLM4.0,
27 CoLM, SHAW, Couple Model and FSM) have been applied at individual station

1 locations on TP to reproduce soil thermo-hydro dynamics (Li et al., 2009; Wang and
2 Shi, 2007; Xiong et al., 2014; Zhang et al., 2012). Simulations of ground temperature
3 and moisture variations are relatively realistic when using observed atmospheric
4 forcing (Guo and Yang, 2010; Luo et al., 2008). The results were improved by setting
5 appropriate permafrost parameters for soil organic matter contents and soil texture
6 properties (Luo et al., 2008; Wang et al., 2007; Xiong et al., 2014). CLM4.0 has also
7 been used to provide future projections of permafrost extent for the whole TP (Guo and
8 Wang, 2013; Guo et al., 2012), and simulates 81% loss of permafrost area by the end of
9 21st century under the A1B greenhouse gas emissions scenario. This raises the question
10 of how reliable the estimate is in comparison with results from other models.

11

12 Simulations of Northern Hemisphere (NH) permafrost area showed large differences
13 amongst Coupled Model Inter-comparison Project (CMIP5) models (Koven et al., 2013;
14 Slater and Lawrence, 2013). Moreover, different diagnostic methods, using either a
15 direct method, which relies on model simulated ground temperatures, or indirect
16 methods inferred from air temperatures and snow characteristics also lead to quite
17 different permafrost areas. Slater and Lawrence (2013) applied two direct methods to
18 nineteen CMIP5 models and found differences of up to $12.6 \times 10^6 \text{ km}^2$ in diagnosed NH
19 permafrost area. Saito (2013) showed that differences in pre-industrial NH continuous
20 permafrost area between direct and indirect methods were around $3 \times 10^6 \text{ km}^2$. This
21 raises the question why different methods arrive at different estimates and which
22 method is better suited.

23

24 A reliable simulation of permafrost extent is important, since permafrost is a
25 comprehensive reflection of soil thermo-hydro dynamics that is hard to measure
26 directly except at sparse observational sites. Further, reliable present-day simulations
27 can contribute to an increased confidence in simulations of future permafrost

1 degradation by these models. We note that this approach provides information on the
2 ability of models on the warmer and physically unique TP permafrost in a NH
3 simulation, hence providing some test of reliability for simulations of present and
4 future global permafrost over TP.

5

6 To date, an examination of the uncertainties in model-derived TP permafrost area has
7 not been attempted. One way of estimating this uncertainty is to explore a single model
8 and to perform a set of sensitivity experiments in which the model parameters are
9 modified (e.g., Dankers et al., 2011; Essery et al., 2013; Gubler et al., 2013). An
10 alternative approach is to explore an ensemble of multiple models where the
11 uncertainty is discussed in terms of the spread among the models (e.g., Koven et al.,
12 2013; Slater and Lawrence, 2013). Here we follow the second approach and examine
13 the uncertainty of TP permafrost simulations by an ensemble of 6 state-of-the-art
14 stand-alone land-surface schemes. The models are from the Permafrost Carbon
15 Network (PCN; <http://www.permafrostcarbon.org/>) and include a broad variety of
16 snow and ground parameters and descriptions, along with a clear experimental design
17 under prescribed observation-based atmospheric forcing. The first focus of our paper is
18 therefore the quantification of the uncertainty in the simulated TP permafrost area due
19 to the models' structural and parametric differences. Further, using time series of soil
20 temperature from the few available TP stations, we discuss the biases in relation to the
21 land surface model description (e.g. soil texture, vegetation and snow cover). We also
22 discuss in the paper the uncertainty due to the different methods to diagnose the TP
23 permafrost area, with 5 different (direct and indirect) methods.

24

25 In section 2 we introduce the different methods used to derive permafrost extent for the
26 TP from LSMs. Section 3 describes the applied model data, the observation-based
27 estimate of TP permafrost map, the method to assess the agreement of simulated versus

1 observation- based estimate of permafrost maps permafrost maps, and ground
2 temperature data to evaluate soil thermal profiles simulated by the models. Results and
3 discussion are presented in sections 4 and 5, and conclusions are summarized in section
4 6.

5

6 **2 Permafrost Diagnosis**

7 We make use of all five major permafrost diagnostic methods promoted in the literature
8 (Slater and Lawrence, 2013; Guo et al., 2012; Guo and Wang, 2013; Wang et al., 2006;
9 Wang, 2010; Nan et al., 2002; Nan et al., 2012; Saito, 2013; Ran et al., 2012; Wang et
10 al., 2006; Jin et al., 2007; Xu et al., 2001; Nelson and Outcalt, 1987). Since the model
11 intercomparison relies on LSMs that are all driven at monthly resolution, the methods
12 we use are tailored, as usual, to reflect the forcing data resolution. The model-derived
13 TP permafrost maps are shown in Figure 1. The modeling spatial domain is not
14 consistent among the models. CLM4.5, CoLM, JULES and UVic cover the whole TP
15 while others (ISBA, LPJ-GUESS) do not (Table 1). We mainly focus on the common
16 modeling region (Figure 1) to discuss differences between models and methods, but
17 also give the results for whole TP for the four models that produce them.

18 In detail, the five methods are:

19

20 1) Temperature in Soil Layers (TSL)

21 The TSL method allows a direct diagnosis of permafrost from modeled soil temperature
22 (Slater and Lawrence, 2013). The standard definition of permafrost is that ground
23 remains at or below 0 °C for at least two consecutive years. Many recent modeling
24 studies (e.g., Guo et al., 2012; Guo and Wang, 2013; Slater and Lawrence, 2013 and
25 references therein), have consistently adapted this for land surface and earth system
26 models by defining a model grid cell as permafrost if the simulated ground temperature
27 (of at least one level in the upper soil) remains at or below 0 °C for at least 24

1 consecutive months. Furthermore, these model-based studies are limited by the
2 maximum soil depth of the models (Table 1). Hence, we analyze the ground
3 temperatures down to a depth of 3 m, which should be satisfactory as this range spans
4 the observed active layer thickness on TP. Data at higher than monthly temporal
5 resolution are not stored by the models in the PCN archive. Therefore TSL diagnosis is
6 calculated from monthly mean soil temperatures, which has been previously
7 demonstrated to be a viable substitute for model-based estimates of permafrost both on
8 TP (Guo et al., 2012; Guo and Wang, 2013), and for the Arctic (Slater and Lawrence,
9 2013).

10

11 2) Mean Annual Ground Temperature (MAGT)

12 Permafrost is detected if the mean annual ground temperature at the depth of zero
13 annual amplitude is at or below 0 °C (Slater and Lawrence, 2013). Some papers use a
14 slightly higher critical temperature, e.g. 0.5 °C (Wang et al., 2006; Wang, 2010; Nan et
15 al., 2002), which has been found to fit TP observations well. Slater and Lawrence (2013)
16 suggested MAGT as an indicator of deeper permafrost. The problem with this
17 definition is that many models have quite shallow soil depth (Table 1), and of course,
18 zero amplitude would require great (actually infinite in steady state) soil depth. For
19 practical purposes, we use MAGT at 3 m depth (the approximate base of the active
20 layer) and the common critical temperature of 0 °C. Although annual ground
21 temperature amplitudes at 3 m depth are still several degrees, they are much smaller
22 than the amplitudes in upper layers (section 4.3). We investigated one model with a
23 larger depth range (CLM4.5; Table 1) in more detail, but found that the results using
24 MAGT at 38 m depth do not significantly change the derived permafrost area.

25

26 3) Surface frost index (SFI)

27 Originally, Nelson and Outcalt (1987) introduced the surface frost index SFI^* , also used

1 in Slater and Lawrence (2013):

$$2 \quad SFI^* = \frac{\sqrt{DDF_a^*}}{\sqrt{DDF_a^*} + \sqrt{DDT_a}} \quad (1),$$

3 Where DDF_a^* and DDT_a are the annual freezing and thawing degree-day sums, both
4 calculated using air temperature (indicated by a subscripts), and with DDF_a^* further
5 modified to correct for the insulating effect of snow cover (indicated by the
6 *superscript). In this way, SFI^* is designed to reflect the ground surface thermal
7 conditions by combining snow insulation effect with air temperature. However, the
8 snow insulation effect alone can not account for the soil structure complexity. So here
9 we calculate surface frost index directly from the ground surface temperature (indicated
10 by s subscripts) (Nan et al., 2012), using an asymmetric sinusoidal annual temperature
11 cycle fitted to the warmest and coldest monthly temperatures (\bar{T}_h, \bar{T}_c) and a frost angle
12 (β) (Nan et al., 2012):

$$13 \quad SFI = \frac{\sqrt{DDF_s}}{\sqrt{DDF_s} + \sqrt{DDT_s}} = \frac{1}{1 + \sqrt{\frac{\beta(\bar{T}_h + \bar{T}_c) + (\bar{T}_h - \bar{T}_c) \sin \beta}{(\beta - \pi)(\bar{T}_h + \bar{T}_c) + (\bar{T}_h - \bar{T}_c) \sin \beta}}} \quad (2),$$

14 Nan et al. (2012) report good results using this surface frost index on TP with values of
15 $SFI \geq 0.5$ to indicate permafrost.

16

17 4) Air frost index (F)

18 Nelson (1987) calculated F from an equation analogous to (2), but using monthly air
19 temperature rather than ground surface temperatures. Where $F \geq 0.5$ defines
20 permafrost. We follow suit and use F to assess the effects of air temperature forcing.
21 Although many authors have criticized F as a permafrost indicator, F has been used in
22 recent work, though in modified forms. For example, Saito (2013) calculated mean
23 annual air temperature (MAAT) as $MAAT = (DDT_a - DDF_a)/365$, where DDT_a

1 and DDF_a , are thawing index and freezing index as defined earlier which means that
2 MAAT in Saito (2013) is a proxy for F.

3

4 5) Mean Annual Air Temperature (MAAT)

5 A critical value of MAAT is often used to derive the southern boundary of permafrost
6 (Ran et al., 2012; Wang et al., 2006; Jin et al., 2007). The $-2\text{ }^{\circ}\text{C}$ isotherm of MAAT has
7 been found to fit well with TP observation- based permafrost maps (Xu et al., 2001).
8 MAAT has been used to compare the air temperature based permafrost area with
9 permafrost areas derived by other methods (Koven et al., 2013; Saito et al., 2013). Note
10 that the calculation method of MAAT in Saito et al. (2013) is slightly different from that
11 used in other works. Here we calculated MAAT traditionally, as the average of 12
12 monthly 2 m air temperatures.

13

14 All the 5 diagnostic methods are summarized in Table 2. The three direct methods (TSL,
15 MAGT, SFI) are based on simulated ground temperatures, while the two indirect
16 methods (F and MAAT) use the prescribed air temperature. SFI is mainly controlled by
17 air temperature and snow cover, but it also depends on how the soil is parameterized, so
18 SFI is somewhat closer to the indirect methods than are TSL and MAGT.

19

20 The 3 methods introduced in the 1980s (SFI, F, MAAT), were designed to map
21 permafrost based on the assumption that the permafrost distribution is related to
22 climatic parameters. Although permafrost processes are directly represented in climate
23 models nowadays, the simulated soil temperatures have considerable errors, and the
24 directly diagnosed permafrost area has model-dependent biases (Koven et al., 2013;
25 Slater and Lawrence, 2013). Therefore the older indirect diagnostic methods are also
26 still very commonly used (e.g., Wang et al., 2006; Jin et al., 2007; Ran et al., 2012; Nan

1 et al., 2012; Slater and Lawrence, 2013; Saito, 2013; Koven et al., 2013). TP permafrost
2 area directly diagnosed from the simulated monthly soil temperatures (TSL) is not
3 superior to the other methods in comparison with the observation-derived permafrost
4 map (Figures 1 and 2). Hence, we consider all the 5 diagnostic methods to quantify the
5 full range of uncertainty in the model-derived permafrost maps.

6

7 Since the forcing air temperatures of LSMs were not the same due to discrepancies in
8 the historical temperature (and precipitation and other forcing fields) datasets used by
9 the individual models (Table 1), we use the indirect methods to quantify forcing
10 differences. If these differences are not too large, we can attribute the differences in the
11 direct method-derived permafrost areas primarily to differences of modeled land
12 surface processes. Across-model and across-method variability is listed in Table 3. As
13 we use fairly small numbers of methods and models, rather than defining uncertainty in
14 terms of standard deviation, we choose to use the full range of values from the
15 simulations and define uncertainty as maximum-minimum values among the models.

16

17 **3 Data and Analysis Approach**

18 **3.1 Data from stand-alone LSMs**

19 Output from six stand-alone LSMs participating in the inter-model comparison project
20 “Vulnerability of Permafrost Carbon to Climate Change”
21 (<http://www.permafrostcarbon.org/>) is analyzed in this study (Table 1). The simulations
22 have been generally conducted for recent decades from 1960 to 2009 using monthly
23 resolution climate forcing input data. Each modeling team was free to choose
24 appropriate driving data sets for climate, atmospheric CO₂, N deposition, disturbance,
25 soil texture, etc., as used in their standard modeling system. Model spin-ups are also
26 different, but they are long enough (around 1 000 years) to ensure that the deep carbon
27 is in equilibrium. The LSMs use different horizontal model resolutions and different

1 soil layer divisions (Table 1).

2

3 Our analysis is based on monthly averages of the driving air temperature and simulated
4 ground temperature. As three models (CoLM, JULES and LPJ-GUESS; Table 1) have
5 shallow soil layers, we restrict our analysis to the common depth range spanning near
6 surface to 3 m. Ground temperatures were linearly interpolated onto the common
7 depths: 0.05, 0.1, 0.2, 0.5, 1, 2, 3 m. Since there is no ground surface temperature output,
8 we linearly extrapolate the top two layers' soil temperatures onto the ground surface.
9 For CLM4.5, CoLM, ISBA and LPJ-GUESS, the first layer soil depth is no deeper than
10 0.01 m and the second layer soil depth is no deeper than 0.05 m. For JULES and UVic,
11 the first layer soil depth is 0.05 m and the second layer soil depth is no deeper than 0.18
12 m. Most TP permafrost work has been post-1980 (Guo and Wang, 2013; Nan et al.,
13 2012), so we choose 1980 as the start of the analysis period. The end is limited to the
14 year 2000 by results from the JULES model (Table 1).

15

16 The LSMs in this study considered the following processes: dynamic vegetation,
17 carbon cycling (Rawlins et al., 2015), snow, near-surface hydrological budget, soil
18 thermal dynamics (Peng et al., 2015) and the treatment of freezing soil. Sophistication
19 in the treatment of these processes varies amongst the models with each having specific
20 parameterizations, In this study we investigate some key schemes and parameters that
21 are important for permafrost simulation: 1) Unfrozen water / phase change. All models
22 calculate soil thermal properties as a function of soil moisture and consider the phase
23 change of water/ice, but CoLM and LPJ-GUESS do not consider transformation to ice
24 of water solute mixtures below 0 °C, which is a key feature in soil freezing and thawing.
25 2) Surface organic layer insulation. Only CLM4.5 and ISBA consider the insulating
26 effect of moss. 3) Soil texture parameterization. The specified fraction of clay and sand
27 in soil differs. LPJ-GUESS specifies the same soil texture for the TP as for the Arctic. 4)

1 Organic soil fraction treatment. The organic content of soil differs among the models.
2 LPJ-GUESS sets the same value for TP as for the more organically rich permafrost of
3 the Arctic. 5) Snow processes. ISBA, LPJ-GUESS and UVic set static snow layers.
4 UVic uses an implicit snow scheme while LPJ-GUESS uses the Bulk-layer scheme,
5 which are both simpler than the dynamic multi-layer snow scheme of some other land
6 models.

7

8 **3.2 TP permafrost observation-based map**

9 Mapping permafrost on TP is challenging due to absence of field observations,
10 especially in the central and western parts where permafrost is widespread. In practice,
11 permafrost maps on TP have been statistical models based on a compilation of earlier
12 maps, aerial photographs, Landsat images and terrain analysis (Ran et al., 2012; Shi et
13 al., 1988; Li and Cheng, 1996; Nan et al., 2002) as well as on some MAGT and MAAT
14 data from the few long-term monitoring sites (Ran et al., 2012; Wang et al., 2006). The
15 classification and therefore the mapping of TP permafrost is not consistent across the
16 different studies (Ran et al., 2012). Thus there is a large spread of observation-based TP
17 permafrost area estimates from $110 \times 10^4 \text{ km}^2$ (Wang et al., 2006) to $150 \times 10^4 \text{ km}^2$ (Shi
18 and Mi, 1988; Li and Cheng, 1996).

19

20 The mostly widely used map by Li and Cheng (1996) has large differences from other
21 maps, and shows excess permafrost in the southeast where permafrost can only exist on
22 extremely cold mountains (Gruber, 2012). The International Permafrost Association
23 (IPA) map (Brown et al., 1997; Heginbottom, 2002) is the most widely used in NH
24 permafrost analysis. However, the IPA map is not well suited for TP because the data
25 and information in this map is based on the map made by Shi et al. (1988) which has not
26 been updated since.

27

1 We use the 1 : 4,000,000 Map of the Glaciers, Frozen Ground and Deserts in China
2 (Wang et al., 2006, hereafter referred to as the “Wang06 map”) as the primary reference.
3 The map is based on MAGT (Nan et al., 2002) with 0.5 °C as the boundary between
4 permafrost and seasonally frozen ground. Nan (2002) fitted a multiple linear regression
5 between latitude, altitude and MAGT, from all 76 TP stations having borehole data, and
6 extrapolated this regression to the whole TP with a 1 km resolution DEM to get the
7 MAGT distribution. The Wang06 map was re-gridded to match the different model
8 resolutions and spatial domain (see “Wang06 map” column in Figure 1), and the
9 different permafrost areas derived from the methods and models are compared with the
10 Wang06 map in Figure 2.

11

12 We emphasize that the Wang06 map is subject to uncertainty as it is based on a
13 relatively sparse set of observations and then statistical extrapolation. Nan et al. (2013)
14 pointed out that permafrost was overestimated in the western TP in both the maps by Li
15 and Cheng (1996) and Wang et al. (2006). However, a better permafrost map covering
16 the whole TP is not available.

17

18 **3.3 Measure of agreement between simulated and Wang06 permafrost** 19 **maps**

20 To evaluate the agreement of simulated permafrost map with the Wang06 map, we
21 calculate the Kappa coefficient (Cohen, 1960; Monserud and Leemans, 1992; Wang,
22 2010), K , which measures the degree of agreement between two maps.

$$23 \quad K = \frac{(s/n - (a_1b_1 + a_0b_0)/n^2)}{(1 - (a_1b_1 + a_0b_0)/n^2)} \quad (3)$$

24 Where the total number of the map points is n , and s is the number of points where
25 simulation and observational estimate agree. The numbers of Wang06 map cells with

1 permafrost is a_1 , and those without are a_0 , and the corresponding simulated map cell
2 numbers are b_1 and b_0 . The calculated K matrix of simulated and Wang06 permafrost
3 maps is presented in Figure 3. Empirically and statistically arbitrary quality values for
4 K have been proposed, e.g. Cohen (1960) suggested that $K \geq 0.8$ signifies excellent
5 agreement, $0.6 \leq K < 0.8$ represents substantial agreement, $0.4 \leq K < 0.6$ represents
6 moderate agreement, $0.2 \leq K < 0.4$ represents fair agreement, while lack of agreement
7 corresponds to $K < 0.2$. There is a sample size issue in estimating the confidence of K
8 and this can be a factor when very small numbers of grid points are available (here this
9 applies to UVic).

10

11 **3.4 Data used to examine model thermal structures**

12 The derived permafrost maps depend on the modeled ground thermal structures.
13 However, field studies on TP are quite limited, and we have only short duration
14 (1996-2000) ground temperature profiles obtained from the GEWEX Asian Monsoon
15 Experiment (GAME)-Tibet (Yang et al., 2003) at three permafrost stations (D66, D105,
16 D110; Figure 1) in the central TP to compare with model results. The three stations are
17 located along the Qinghai-Tibet Highway. D66 station is in the front edge of alluvial
18 fan, with almost no vegetation. The soil is mainly composed of gravels, sands and
19 pebbles. D110 is in the southern bank of ZhaJiaZangBu River. The ground is a wetland
20 covered with short-stature emergent vegetation. The upper layer soil is composed of
21 coarse and fine sand. The lower soil layer is mainly composed of fine sand. D105 is in
22 the northern side of the Tanggula Mountain range. The ground surface is relatively flat,
23 covered with plateau meadow. The soil is composed of both coarse and fine sand. The
24 vertical profile of observed soil temperature of D66 extends from 0.04 m to 2.63 m, of
25 D110 from 0.04 m to 1.8 m, and of D105 from 0 to 3 m. However the data continuity of
26 the top layer temperature in D105 is not good. To examine modeled ground
27 temperatures, we present the top (0.04 m) and deeper (2.63 m or 3 m) soil layer

1 temperatures (modeled temperatures were weighted bi-linear interpolated onto the
2 station locations) in Figure 4 and Table 4. We also give a short description of the sites
3 vegetation and soil texture information, both from observation and models.

4

5 We also analyze monthly air and ground temperatures in a selected area in the western
6 TP (33° - 36° N, 82.5° - 85.5° E, Figure 1) to examine across-model differences
7 (Figure 5). The air temperature is also different among the models, especially in winter
8 season, though the differences are much smaller than soil temperatures differences. As
9 this region is the coldest part of TP (according to the annual mean air temperature) the
10 permafrost is widely distributed, and the active layer thickness is less than 3 m.
11 However, TSL method derived permafrost areas vary significantly among the models in
12 this area (Figure 1). Despite the lack of any ground temperature observations in this
13 area, the definite presence of permafrost makes it useful to look at the ground thermal
14 structure of each model as well as their differences as a means of interpreting the
15 calculated permafrost areas.

16

17 **4 Results and Discussion**

18 **4.1 Uncertainties in air-temperature-derived permafrost area**

19 Air temperature-derived permafrost maps are investigated with the two indirect
20 methods, F and MAAT. Figures 1 and 2 compare both Wang06 and model-derived
21 permafrost maps, and show that F produces consistently excessive permafrost area
22 compared with MAAT. That is because the empirical threshold of -2°C for MAAT fits
23 well with TP observations (Xu et al., 2001), while $F \geq 0.5$ is a theoretical assumption,
24 which has been reported to overestimate permafrost area (Nelson and Outcalt, 1987;
25 Slater and Lawrence, 2013). Accordingly, Figure 3 shows that F-derived permafrost is
26 less consistent with Wang06 map (model average $K = 0.3$ for the common region) than
27 MAAT-derived permafrost area ($K = 0.5$).

1

2 Across-model variability (Table 3) for the MAAT-based method is $14 \times 10^4 \text{ km}^2$ and for
3 the F-based method is $17 \times 10^4 \text{ km}^2$, equivalent to about 14 % ~ 17 % of the Wang06
4 permafrost area inside the common modeling region ($101 \times 10^4 \text{ km}^2$). This variability is
5 much smaller than the 56% calculated by Slater and Lawrence (2013) for the CMIP5
6 models with the SFI* method for NH permafrost area. The relatively smaller difference
7 among the models here is because, although the temperature forcing was not identical
8 among models, the mean annual air temperature and its spatial variability in the
9 permafrost region are quite similar (between $-6 \text{ }^\circ\text{C}$ and $-8 \text{ }^\circ\text{C}$). Since the differences in
10 permafrost extent using the air temperature based indirect methods are relatively small,
11 the differences in the direct method derived extents can primarily be attributed to the
12 LSMs structural and parametric differences.

13

14 **4.2 Uncertainties in model-derived permafrost area**

15 There is a large across-model variability of permafrost area derived from direct
16 methods (TSL, MAGT and SFI) (Figures 1, 2; $111 \sim 120 \times 10^4 \text{ km}^2$; Table 3) and it is
17 similar for all the 3 diagnosis methods. This across-model variability is much larger
18 than the variability using the indirect methods discussed in Section 4.1, and is
19 equivalent to 110-112% of Wang06 permafrost area for the common modeling region.
20 CMIP5 across-model variability derived from TSL in NH permafrost area was similarly
21 large (Slater and Lawrence, 2013; Koven 2013). Clearly this points to large
22 across-model differences in ground thermal structures.

23

24 The across-method (TSL, MAGT and SFI) variability in permafrost area (Figures 1, 2;
25 Table 3) is very variable between models: UVic and LPJ-GUESS have smallest ranges
26 (up to $9 \times 10^4 \text{ km}^2$), while CoLM has the largest ($87 \times 10^4 \text{ km}^2$) (Table 3), near to the
27 total permafrost area of the common region. Thus the across-direct method range is

1 similar to the across-model range. Slater and Lawrence (2013) also emphasized the
2 variable across-method variability for NH permafrost area between models, however
3 Saito (2013) showed insignificant variability across both direct and indirect methods
4 for derived pre-industrial NH continuous permafrost area.

5

6 **4.3 Model evaluation based on K and ground temperature profile**

7 A good land surface model should adequately simulate the seasonal and annual ground
8 temperature profiles. Hence one quality test for a model is that it should be able to
9 produce ‘good’ permafrost maps, which we define as agreement with the
10 observation-based map, based on all the three direct diagnostic methods. The applied
11 criterion is the kappa coefficient K (section 3.3), and we limit discussion to the K
12 associated with TSL, MAGT and SFI, which are calculated with simulated soil
13 temperatures. If we take the (arbitrary) threshold $K \geq 0.4$ (indicating “moderate
14 agreement”), then no model passes this test for the common simulation region, while
15 reducing the threshold to $K \geq 0.2$ (“fair agreement”) allows most models and methods
16 to pass while UVic stands out as a clear failure (Figure 3).

17

18 If the criterion for acceptable model bias is $\leq \pm 2.0$ °C, then simulations of mean annual
19 ground temperatures from most models (CLM4.5, CoLM, ISBA and JULES) agree
20 with the observations, but only the simulation of seasonal cycle amplitude of one model
21 (ISBA) is consistent with the limited observations. However, if the criterion is bias \leq
22 ± 1.0 °C, then no model agrees with observations for neither mean annual ground
23 temperature nor the seasonal cycle amplitude (Figure 4, Table 4).

24

25 We now look at the performance of the 2 models with larger biases in mean annual
26 ground temperature: LPJ-GUESS and UVic. LPJ-GUESS simulated too cold (by more
27 than 3 °C) mean annual ground temperatures for both the surface and deeper layers

1 (Figure 4, Table 4). The summer temperatures simulated by the model in the surface
2 layers are especially cold, with maximum temperatures lower than observation by 8 °C
3 (Figures 4a, c) and its ground temperature amplitude is substantially underestimated
4 (Table 4), which must greatly limit the summer thaw depth. This cold soil results in
5 substantial overestimation of permafrost area ($119 \sim 131 \times 10^4 \text{ km}^2$; Table 3, Figure 2)
6 with small across-method variability.

7

8 UVic simulates a soil thermal state that is the warmest among the models, with the
9 simulated mean annual ground temperature at D66 surpassing observation by more
10 than 7 °C (Figure 4, Table 4). If the observational sites are representative then the
11 generally too warm ground temperature in UVic is the reason for the extremely small
12 simulated permafrost area ($8 \times 10^4 \text{ km}^2$; Table 3, Figure 2) with all direct methods, and
13 hence to no across-method variability, and poor agreement with the Wang06 permafrost
14 map ($K < 0.1$; Figure 3).

15

16 **4.4 Method comparison based on K and ground temperature profile**

17 Permafrost maps derived using MAGT and SFI often show larger area than TSL
18 (Figure 2), with generally better agreement with the Wang06 map (Figure 3). The
19 MAGT method simply defines a grid as permafrost as long as its 3 m mean annual
20 ground temperature is colder than 0 °C, and a permafrost threshold value of $\text{SFI} \geq 0.5$
21 also only requires the mean annual ground surface temperature is lower than 0 °C (Nan,
22 2012). Figure 4 and Figure 5 show most models meet these criteria. However, assuming
23 that the site observations are representative, the simulated mean annual ground
24 temperatures of both surface and deeper soil layers often have obvious biases ($\geq \pm 1 \text{ }^\circ\text{C}$)
25 in all the models (Figure 4 and Table 4).

26

27 In general, model-derived permafrost distribution using the TSL method shows little

1 agreement with the Wang06 map (Figures 1 - 3). In contrast with MAGT and SFI
2 methods, the TSL method requires adequate simulation of both mean annual ground
3 temperature and the seasonal cycle at monthly resolution (Figure 4, Table 4). This
4 means that the TSL method is more susceptible to model errors, but it offers a more
5 comprehensive insight into land model processes. CoLM is an extreme example of how
6 a simulated permafrost map can be totally incorrect due to small errors in seasonal
7 ground temperature. CoLM simulates nearly no TSL-derived permafrost (Figures 1, 2),
8 accounting for much of the large across-model and across-method variability (Table 3).
9 We investigate both the air and ground temperature (Figure 5) of the selected region
10 (the region shown in Figure 1), which is the coldest part of TP and should be permafrost.
11 CoLM simulates no permafrost in the selected region despite CoLM having lower
12 mean annual ground temperatures for the 3 m layer than many other models (ISBA,
13 CLM4.5 and JULES) (Figure 5). However, CoLM simulates a larger seasonal
14 amplitude than CLM4.5 and ISBA (Figure 5), so that, in the western TP, the monthly
15 maximum 3 m ground temperatures in CoLM always surpasses 0 °C by around 0.2 °C
16 (Figure 5c) precluding it being classified as permafrost with the TSL method.

17

18 **5 Main processes causing ground temperature discrepancies**

19 As discussed in Sect. 4, the most noticeable ground temperature discrepancies among
20 the 6 models are the underestimation of soil temperature by LPJ-GUESS and the
21 overestimation of soil temperature by UVic, which lead to the largest biases in
22 simulated permafrost area. There are many other, rather subtle, potential model
23 discrepancies that we do not investigate in detail here. One example is the
24 overestimation of the amplitude of the seasonal temperature cycle at deep depths in
25 several models (Figures 4b and 4d; Table 4). Table 4 also shows that the observed
26 vegetation and soil texture are mis-matched by all the models at each of the stations.
27 Although it is a common problem to compare grid cell results against site data, model
28 description of vegetation and soil texture is too simplified.

1

2 To help elucidate the causes of ground temperature discrepancies associated with soil
3 processes we also inspect snow depth and vertical ground temperature gradients. We
4 use the Long Time Series Snow Dataset of China (Che et al., 2008)
5 (<http://westdc.westgis.ac.cn>) to examine the modeled snow depth. The complete
6 dataset is composed of SMMR (1978-1987), SSM/I (1987-2008) and AMSR-E
7 (2002-2010). According to Wang et al. (2013), the snow depth pattern and the
8 significant seasonal snow characteristics of the satellite data are consistent with those
9 of station data in most of our common TP region. The satellite data are different from
10 station data on the southeast of TP (Wang et al., 2013), however, our analyzed common
11 region does not include this part of TP. Thus this satellite data is reliable in this study.
12 Here we use the data of SMMR and SSM/I to produce the winter (DJF) climatological
13 distribution of 1980-2000 (Figure 6). Furthermore, we follow Koven et al. (2013) and
14 calculated two vertical gradients to isolate processes: from the atmosphere to ground
15 surface (Figure 7) and from ground surface to deeper soil (at 1 m depth) (Figure 8).
16 While the first one is mainly controlled by the snow insulation, the latter is mainly
17 determined by soil hydrology, latent heat and thermal properties. Important factors that
18 influence the ground thermal structure are compared in Table 5. Since several models
19 produce incomplete or not directly comparable output, we restrict ourselves to a
20 qualitative assessment here.

21

22 The LPJ-GUESS simulated underestimation of soil temperature is not caused by a bias
23 in the surface air temperature forcing (Figure 5, Table 4). Instead, this bias may be due
24 to many factors such as inappropriate prescriptions of soil thermal properties, poor
25 representation of soil hydrology, mis-match of vegetation types, and weak coupling of
26 soil water and vegetation cover. Figure 8 shows that the soil temperatures increase with
27 depth, but LPJ-GUESS has a much smaller temperature gradient between the surface
28 and the 1 m deep soil (0-2 K) than the other models. This suggests a different (larger)

1 winter soil thermal conductivity probably associated with a high soil porosity and water
2 content. LPJ-GUESS specifies the same soil texture for the TP as for the Arctic, which
3 is mostly clay-like (Table 4). Clay has high water retention capacity. Many studies have
4 reported that the soil on TP is immature, with coarser particles than typical for Arctic
5 permafrost and with much less organic matter. Inappropriate soil texture classification
6 will affect the simulated ground thermal structure. LPJ-GUESS underestimates the
7 surface and top soil temperatures particularly in summer (Figures 4a, c, 5).
8 Precipitation and hydrological processes determine the vertical profile of soil water
9 content which can change the fraction of water and ice retained in different soil layers
10 and influence soil thermal conduction. The energy required to melt the high water (ice)
11 content in the surface soil layers in summer appears to lead to underestimated low
12 summer temperatures compared with other models, and a phase lag in summer
13 warming (Figures 4a and 4c).

14

15 In addition, LPJ-GUESS shows a similarly thick snow depth in the western part of
16 Tibetan Plateau as CLM4.5 and CoLM (Figure 6), but does not show as large surface a
17 temperature offset as those two models (Figure 7). That is because LPJ-GUESS has a
18 fixed snow density (362 kg/m^3) which is higher than used in other models, and a
19 relatively simple Bulk-layer snow scheme, with one static snow layer, unlike the
20 dynamic multi-layer snow scheme of CLM4.5 and CoLM (Table 5).

21

22 UVic uses the same climate forcing as CLM4.5 (Table 1), but simulates much warmer
23 ground temperatures than other models. In contrast with the other models, UVic has no
24 snow cover in winter (Figure 6), which is consistent with grid cell surface albedo being
25 year-round at values between 0.15-0.35. The simulated snow depth is derived from the
26 prescribed winter precipitation, and the model's snow, energy and water balances. The
27 lack of snow over TP in UVic likely indicates removal by sublimation. A too low snow

1 albedo makes the snow gain energy that is lost through sublimation. Since it takes more
2 energy to sublimate snow than it does to melt it, the latent heat flux should be, and is
3 (not shown) higher in UVic than other models. However, despite the apparent snow
4 sublimation - which should cool the soil, the ground surface temperatures in UVic are
5 warmer than in all the models. The large absorption of short wave radiation allowed by
6 the year-round low albedo provides this heat and is sufficient for there to be very little
7 permafrost simulated by UVic for the TP.

8

9 ISBA, and especially JULES stand out from other models in their calculated winter
10 temperature offsets: ground surface temperatures are colder than the driving air
11 temperatures over much of the simulated region (Figure 7). Snow (Figure 6) and
12 vegetation cover would normally be expected to provide insulation, making soil
13 warmer than air temperatures in winter. However, we observe that the snow depths
14 from ISBA and JULES are not very thick (<10 cm) in most places on TP (Figure 6).
15 Figure 9 shows the temperature offset between ground surface and air temperature as a
16 function of snow depth. By inspection we note that there is different behavior for snow
17 depths thinner and thicker than 4 cm. For snow depth > 4 cm, most negative offsets
18 disappear in ISBA and JULES, which means that the ground surface temperature is
19 warmer than air temperature for snow depth larger than 4 cm. For snow depth < 4 cm,
20 the ground surface temperature of much of the region is colder than air temperature in
21 ISBA and JULES, which indicates the cooling effect of thin snow. The very small or
22 slightly negative temperature offset for thin snow is also seen in the other models. Of
23 course, the strength of this effect depends on the individual model's
24 simulation/parameterization of the snow processes (such as sublimation, evaporation,
25 melting). The thin snow mechanism is also confirmed by the weak insulation effect in
26 Figure 10.

27

1 **6 Robustness of the results**

2 **6.1 Choice of thresholds in the methodologies**

3 In Sect. 4 we used the most commonly applied threshold of each method, based on the
4 empirical findings from previous studies, to compare models and methods. However,
5 the thresholds themselves have the potential to affect the results. To reduce the latent
6 uncertainties in terms of the methodologies, we also examine the sensitivity of
7 permafrost area for different thresholds (Table 2), calculating changes in the permafrost
8 area (Table 3) for a range of thresholds for each method (i.e., $-3\text{ °C} < \text{MAAT} < 0\text{ °C}$;
9 $0.4 < F < 0.6$; $0.4 < \text{SFI} < 0.6$; $0\text{ °C} < \text{MAGT} < 0.5\text{ °C}$).

10

11 Generally, when the permafrost definition requires colder climate, the derived
12 permafrost area becomes smaller. The across-threshold uncertainty (Table 3) is similar
13 for different models. But the across-threshold uncertainty with SFI varies greatly
14 among models, $23 \sim 105 \times 10^4 \text{ km}^2$, which is due to the seasonal amplitude of ground
15 surface temperatures it requires. This is illustrated in Figure 5 where UVic and
16 LPJ-GUESS have a relatively small seasonal amplitude of ground surface temperature,
17 which corresponds to their small across-threshold variability for SFI derived area in
18 Table 3.

19

20 The across-model uncertainty is highly consistent even with different thresholds for
21 each method (Table 3 final column). Thus it seems changing the thresholds does not
22 affect one key point in our paper: that across-model uncertainties using direct methods
23 are much larger than using indirect ones. Large across-model uncertainties using direct
24 methods imply that differences among these land surface processes are worthy of
25 investigation.

26

1 **6.2 Model settings**

2 The lowest soil boundary is a critical uncertainty affecting the simulation of permafrost
3 (Nicolsky et al., 2007). The common boundary of 3 m soil depth may produce
4 uncertainties in the derived permafrost area. Three (CLM4.5, ISBA, UVic) of the six
5 models extended the soil to deeper depths (Table 1), which provides insight on this
6 issue. As UVic does not do a reasonable simulation of snow cover and ground
7 temperature, we feel it is not necessary to include this model in the discussion here.
8 Based on results from CLM4.5 and ISBA, the permafrost area calculated from MAGT
9 at 3 m and at 10 m only changes by $1 \times 10^4 \text{ km}^2$. For results from CLM4.5, the areas
10 calculated from MAGT at 20 m and 30 m do not change from the one calculated at 10 m.
11 This is due to MAGT only considering annual mean soil temperature, not the seasonal
12 cycle. This is consistent with the finding that the across-threshold uncertainty for
13 MAGT-derived permafrost area is quite small (Table 3). However, the derived
14 permafrost area with the TSL method improves when soil depth used for calculation is
15 increased from 3 m to 5 m (Table 6). This sensitivity is because TSL requires
16 information on the seasonal cycle of soil temperature. In other words, results of TSL
17 method are sensitive to the active layer dynamics. The permafrost on TP is usually
18 much warmer and has a deeper active layer than found in continuous permafrost of the
19 arctic and boreal region. Hence deeper soil layers would be well suited for TP
20 permafrost simulation. A shallow column in a permafrost model can cause problems in
21 the simulation of the degradation of warm permafrost (near 0°C), which is expected for
22 projections of future climate warming (Lawrence et al., 2008). In addition, Alexeev et
23 al. (2007) pointed out that deep soil configuration can improve the simulation of
24 seasonal and even annual cycle of shallow layers. Nicolsky et al. (2007) recommend a
25 soil column of at least 80 m for models applied to permafrost regions.

26

27 Soil layer discretization and spatial resolutions are different among the six models
28 (Table 1). In this study we linearly interpolated and extrapolated the soil temperatures

1 onto the standard layers (Sect. 3.1). The impact of ground surface temperature
2 extrapolation was found to be small by comparing Figures 7 and 8 with those made
3 using temperatures at 5 cm depth (not shown), with both geographical patterns and
4 widespread negative surface temperature offsets in ISBA and JULES. We re-gridded
5 the Wang06 map onto each model's spatial resolution to evaluate the models
6 objectively. This leads to an error bar estimate of half a grid cell area, up to 20×10^4
7 km^2 , which is half of the spread of observation area estimates (Sect. 3.2). Daily and
8 hourly temperature data may make some differences to the permafrost extent map, but
9 the diurnal cycle wave decays at shallower soil depths than the deepest model layer.

10

11 **7 Summary and Conclusions**

12 Results of this model intercomparison quantify, for the first time, the uncertainties of
13 model derived permafrost area on the Tibetan Plateau (TP). The uncertainties stem
14 from across-model and across-diagnostic method variability as well as historic climate
15 data uncertainties. According to the agreement of the air temperature based diagnostic
16 methods (MAAT and F), we found lower uncertainty in permafrost area associated with
17 air temperature forcing (99 to $135 \times 10^4 \text{ km}^2$) in comparison with the uncertainty (1 to
18 $128 \times 10^4 \text{ km}^2$) associated with the simulation of soil temperature used in the other three
19 diagnostic methods (TSL, MAGT, and SFI). The observation-based Wang06
20 permafrost area is $101 \times 10^4 \text{ km}^2$.

21

22 Most models in this study produced permafrost maps in better agreement with the
23 Wang06 map using the MAGT and SFI methods rather than with the TSL method. But
24 this does not mean that the models simulate permafrost dynamics correctly. Although
25 most models can capture the threshold value of MAGT and SFI, their ground
26 temperatures still show various biases, both in the mean annual value and the seasonal
27 variation. Therefore, most models produce worse permafrost maps with the TSL

1 method. The TSL method is a more demanding, and to date, elusive target.

2

3 Modeled snow depth and surface and soil temperature offsets vary widely amongst the
4 models. If the observation sites for soil temperature are representative, then
5 LPJ-GUESS and UVic have substantial biases in their soil temperature simulations,
6 mainly attributable to inappropriate description of the surface (vegetation, snow cover)
7 and soil properties (soil texture, hydrology). Other models (ISBA, JULES) show biases
8 in the simulation of winter soil temperature.

9

10 Further evaluation of model results from the permafrost-RCN is underway for TP that
11 examines permafrost temperature, active layer thickness and carbon balance under
12 present and future climate forcing. We also plan to complement this model
13 intercomparison study by an uncertainty quantification analysis of key model
14 parameters (e.g. improved vegetation and snow albedo, soil colors, etc) with the CoLM
15 model. However, a crucial requirement for this is much better data availability allowing
16 for better spatial coverage across the TP in the evaluation of simulated ground
17 temperature profiles. Under the Chinese Scientific Foundation Project “Permafrost
18 Background Investigation on the Tibetan Plateau” (No. 2010CB951402), a series of
19 new stations have been established, especially in the depopulated zone. More ground
20 truth data will be published in the near future, which will also be assimilated in a new
21 observation-based permafrost map.

22

23 **Acknowledgements**

24 This study was supported by the Permafrost Carbon Vulnerability Research
25 Coordination Network, which is funded by the National Science Foundation. Any use
26 of trade, firm, or product names is for descriptive purposes only and does not imply
27 endorsement by the U.S. Government. E.J.B. was supported by the Joint UK

1 DECC/Defra Met Office Hadley Centre Climate Programme (GA01101) and the
2 European Union Seventh Framework Programme (FP7/2007-2013) under grant
3 agreement n °282700. This research was also sponsored by Chinese foundations: (1) the
4 National Basic Research Program of China (Grant No. 2015CB953600), (2) the
5 National Science Foundation of China (Grant No. 40905047), (3) the National Natural
6 Science Foundation of China (Grant No.41275003), and (4) the National Natural
7 Science Foundation of China (Grant No.41030106). In addition, Bertrand Decharme
8 and Christine Delire were supported by the French Agence Nationale de la Recherche
9 under agreement ANR-10-CEPL-012-03.

10

11

1 **References**

- 2 Alexeev, V., Nicolsky, D., Romanovsky, V., and Lawrence, D.: An evaluation of
3 deep soil configurations in the CLM3 for improved representation of permafrost,
4 *Geophys. Res. Lett.*, **34**, L09502, doi:10.1029/2007GL029536, 2007.
- 5 Avis, C.A.: Simulating the present-day and future distribution of permafrost in the
6 UVic Earth System Climate Model, Dissertation, University of Victoria, Canada,
7 274pp, 2012.
- 8 AWFA: Data format handbook for AGRMET,
9 Available online: http://www.mmm.ucar.edu/mm5/documents/DATA_FORMAT_HANDBOOK.pdf (accessed on January 20, 2010), 2002.
- 10 T_HANDBOOK.pdf (accessed on January 20, 2010), 2002.
- 11 Best, M.J., and 16 co-authors: The Joint UK Land Environment Simulator(JULES),
12 model description—Part 1: energy and water fluxes, *Geosci.Model. Dev.*, 4,
13 677–699. doi:10.5194/gmd-4-677-2011, 2011.
- 14 Brown, J., Ferrians, O., Heginbottom, J., and Melnikov, E.: Circum-Arctic map of
15 permafrost and ground-ice conditions, US Geological Survey Reston, 1997.
- 16 Che, T., Li, X., Jin, R.: Armstrong R, Zhang TJ, 2008. Snow depth derived from passive
17 microwave remote-sensing data in China, *Annals of Glaciology*, 49:145-154,
18 2008.
- 19 Cohen, J.: A Coefficient of Agreement for Nominal Scales, *Educational and*
20 *Psychological Measurement*, 20 (1), 37-46, 1960.
- 21 Cheng, G., and Jin, H.: Permafrost and groundwater on the Qinghai-Tibet Plateau and in
22 northeast China[J], *Hydrogeology Journal*, 21(1): 5-23, 2013.
- 23 Dai, Y., et al.: The Common Land Model (CLM), *Bull. Am. Meteorol. Soc.*, 84,
24 1013–1023, doi:10.1175/BAMS-84-8-1013, 2003.
- 25 Dankers, R., Burke E. J., and Price, J.: Simulation of permafrost and seasonal thaw
26 depth in the JULES land surface scheme, *The Cryosphere*, 5, 773-790,
27 doi:10.5194/tc-5-773-2011, 2011.
- 28 Decharme, B., Boone, A., Delire, C., and Noilhan, J.: Local evaluation of the
29 Interaction between Soil Biosphere Atmosphere soil multilayer diffusion scheme
30 using four pedo-transfer functions, *J. Geophys. Res.-Atmos.*, 116,
31 D20126,doi:10.1029/2011JD016002, 2011.
- 32 Dörfer, C., Kühn, P., Baumann, F., He, J., and Scholten, T.: Soil organic carbon pools
33 and stocks in permafrost-affected soils on the Tibetan Plateau[J], *PloS one*, 8(2):
34 e57024, doi:10.1371/journal.pone.0057024, 2013.
- 35 Essery, R., Morin, S., Lejeune, Y., and Ménard, C. B.: A comparison of1701snow

- 1 models using observations from an alpine site, *Adv. WaterResour.*, 55, 131–148,
2 doi:10.1016/j.advwatres.2012.07.013, 2013.
- 3 Gerten, D., Schaphoff, S., Haberlandt, U., Lucht, W., and Sitch, S., Terrestrial
4 vegetation and water balance: Hydrological evaluation of adynamic global
5 vegetation model, *J. Hydrol.*, 286, 249–270, 2004.
- 6 Gruber, S.: Derivation and analysis of a high-resolution estimate of global permafrost
7 zonation, *The Cryosphere*, Volume 6, Issue 1, pp. 221-233, 6, 221-233, 2012.
- 8 Gubler, S., Endrizzi, S., Gruber, S., and Pursves, R. S.: Sensitivities and uncertainties
9 of modeled ground temperatures in mountain environments[J], *Geoscientific*
10 *Model Development Discussions*, 6(1): 791-840, 2013.
- 11 Guo, D., and Yang, M.: Simulation of Soil Temperature and Moisture in Seasonally
12 Frozen Ground of Central Tibetan Plateau by SHAW Model, *Plateau Meteorology*,
13 29 (6), 1369-1377, 2010.
- 14 Guo, D., Wang, H., and Li, D.: A projection of permafrost degradation on the Tibetan
15 Plateau during the 21st century, *Journal of Geophysical Research: Atmospheres*
16 (1984–2012), 117, D05106, doi:10.1029/2011JD016545, 2012.
- 17 Guo, D., and Wang, H.: Simulation of permafrost and seasonally frozen ground
18 conditions on the Tibetan Plateau, 1981–2010, *Journal of Geophysical Research:*
19 *Atmospheres*, 118, 5216-5230, 2013.
- 20 Heginbottom, J.: Permafrost mapping: a review, *Progress in Physical Geography*, 26,
21 623-642, 2002.
- 22 Hillel, D.: *Environmental soil physics: Fundamentals, applications, and environmental*
23 *considerations [M]*, Academic Press, New York, USA, 1998.
- 24 IPCC 2013 *Climate change 2013: The Physical Science Basis Contribution of Workin*
25 *g Group I to the Fifth Assessment Report of the Intergovernmental Panel on Cli*
26 *mate Change*, Cambridge University Press, Cambridge.
- 27 Ji, D., Wang, L., Feng, J., Wu, Q., Cheng, H., Zhang, Q., Yang, J., Dong, W., Dai, Y.,
28 Gong, D., Zhang, R.-H., Wang, X., Liu, J., Moore, J. C., Chen, D., and Zhou, M.:
29 Description and basic evaluation of Beijing Normal University Earth System
30 Model (BNU-ESM) version 1, *Geosci. Model Dev.*, 7, 2039-2064,
31 doi:10.5194/gmd-7-2039-2014, 2014.
- 32 Jin, H., Yu, Q., Lü, L., Guo, D., He, R., Yu, S., Sun, G., and Li, Y.: Degradation of
33 permafrost in the Xing'anling Mountains, Northeastern China, *Permafrost and*
34 *Periglacial Processes*, 18, 245-258, 2007.
- 35 Koven, C., Riley, W., and Stern, A.: Analysis of permafrost thermal dynamics and
36 response to climate change in the CMIP5 Earth System Models, *Journal of*
37 *Climate*, 26, 1877-1900, 2013.

- 1 Lawrence, D., and Slater, A.: A projection of severe near - surface permafrost
2 degradation during the 21st century, *Geophysical Research Letters*, 32, L24401,
3 doi:10.1029/2005GL025080, 2005.
- 4 Lawrence, D., Slater A., Romanovsky V., and Nicolsky D.: The sensitivity of a model
5 projection of near-surface permafrost degradation to soil column depth and
6 inclusion of soil organic matter, *J. Geophys. Res.*, 113, F02011,
7 doi:10.1029/2007JF000883, 2008.
- 8 Li, Q., Sun, S., and Dai, Q.: The numerical scheme development of a simplified frozen
9 soil model, *Advances in Atmospheric Sciences*, 26, 940-950, 2009.
- 10 Li, S., and Cheng, G.: *Map of Frozen Ground on Qinghai -Xizang Plateau*, Lanzhou:
11 Gansu Culture Press, 1996.
- 12 Li, S., Gao, S., Yang, P., and Chen, H.: Some problems of freeze-thaw desertification in
13 the Qinghai-Tibetan Plateau: a case study on the desertification regions in the
14 western and northern Tibet[J], *J Glaciol Geocryol*, 27(4): 476-485, 2005.
- 15 Li, Z., Tang, P., Zhou, J., Tian, B., Chen, Q., and Fu, S.: Permafrost environment
16 monitoring on the Qinghai-Tibet Plateau using time series ASAR images[J],
17 *International Journal of Digital Earth*, DOI:10.1080/17538947.2014.923943,
18 2014.
- 19 Luo, S., Lv, S., Zhang, Y., Hu, Z., Ma, Y., Li, S., and Shang, L.: Simulation analysis on
20 land surface process of BJ site of central Tibetan Plateau Using CoLM, *Plateau
21 Meteorology*, 27, 259-271, 2008.
- 22 McGuire, D., et al.: An retrospective assessment of the vulnerability of permafrost
23 carbon in the earth system: Comparison of dynamics among process-based models,
24 in preparation, 2014.
- 25 Meissner, K.J., Weaver, A.J., Matthews, H.D., and Cox, P.M.: The role of land-surface
26 dynamics in glacial inception: A study with the UVic earth system model, *Clim.
27 Dyn.*, 21, 515-537, 2003.
- 28 Monserud, R., and Leemans, R.: Comparing global vegetation maps with the Kappa
29 statistic, *Ecological Modelling*, 62, 275-293, 1992.
- 30 Nan, Z., Huang, P., and Zhao, L.: Permafrost distribution modeling and depth
31 estimation in the Western Qinghai-Tibet Plateau, *Acta Geographica Sinica*, 68,
32 318-327, 2013.
- 33 Nan, Z., Li, S., and Liu, Y.: Mean annual ground temperature distribution on the
34 Tibetan Plateau: permafrost distribution mapping and further application, *Journal
35 of Glaciology and Geocryology*, 24, 142-148, 2002.
- 36 Nan, Z., Li, S., Cheng, G., and Huang, P.: Surface frost number model and its
37 application to the Tibetan plateau, *Journal of Glaciology and Geocryology*, 34,

- 1 89-95, 2012.
- 2 Nelson, F., and Outcalt, S.: A computational method for prediction and regionalization
3 of permafrost, *Arctic and Alpine Research*, 19(3), 279-288, 1987.
- 4 Nicolsky, D. J., V. E. Romanovsky, V. A. Alexeev, and D. M. Lawrence: Improved
5 modeling of permafrost dynamics in a GCM land-surface scheme, *Geophys. Res.*
6 *Lett.*, 34, L08501, doi:[10.1029/2007GL029525](https://doi.org/10.1029/2007GL029525), 2007.
- 7 Oleson, K.W., Lawrence, D.M., Bonan, G.B., Drewniak, B., Huang, M., Koven, C.D.,
8 Levis, S., Li, F., Riley, W.J., Subin, Z.M., Swenson, S.C., Thornton, P.E., Bozbiyik,
9 A., Fisher, R., Kluzek, E., Lamarque, J.-F., Lawrence, P.J., Leung, L.R., Lipscomb,
10 W., Muszala, S., Ricciuto, D.M., Sacks, W., Sun, Y., Tang, J., Yang, Z.L.:
11 Technical description of version 4.5 of the Community Land Model (CLM).
12 NCAR Technical Note NCAR/TN-503+STR, doi: [10.5065/D6RR1W7M](https://doi.org/10.5065/D6RR1W7M), 2013.
- 13 Peng, S., Ciais, P., Krinner, G., Wang T., Gouttevin I., McGuire A.D., Lawrence D.,
14 Burke E., Chen X., Delire C., Koven C., MacDougall A., Rinke A., Saito K.,
15 Zhang W., Alkama R., Bohn T.J., Decharme B., Hajima T., Ji D., Lettenmaier, D.P.,
16 Miller, P.A., Moore, J.C., Smith, B., and Sueyoshi, T.: Simulated high-latitude soil
17 thermal dynamics during the past four decades, *The Cryosphere Discuss.*, 9,
18 2301–2337, doi:[10.5194/tcd-9-2301-2015](https://doi.org/10.5194/tcd-9-2301-2015), 2015.
- 19 Qin, J., Yang, K., Liang, S., Zhang, H., Ma, Y., Guo, X., and Chen, Z.: Evaluation of
20 surface albedo from GEWEX - SRB and ISCCP - FD data against validated
21 MODIS product over the Tibetan Plateau, *Journal of Geophysical Research:*
22 *Atmospheres* (1984–2012), 116, D24116, doi:[10.1029/2011JD015823](https://doi.org/10.1029/2011JD015823), 2011.
- 23 Ran, Y., Li, X., Cheng, G., Zhang, T., Wu, Q., Jin, H., and Jin, R.: Distribution of
24 permafrost in China: An overview of existing permafrost maps, *Permafrost and*
25 *Periglacial Processes*, 23, 322-333, 2012.
- 26 Rawlins, M.A., McGuire, A.D., Kimball, J.S., Dass, P., Lawrence, D., Burke, E., Chen,
27 X., Delire, C., Koven, C., MacDougall, A., Peng, S., Rinke, A., Saito, K., Zhang,
28 W., Alkama, R., Bohn, T.J., Ciais, P., Decharme, B., Gouttevin, I., Hajima, T., Ji,
29 D., Krinner, G., Lettenmaier, D.P., Miller, P.A., Moore, J.C., Smith, B., and
30 Sueyoshi, T.: Assessment of Model Estimates of Land-Atmosphere CO₂
31 Exchange Across Northern Eurasia, *Biogeosciences*, 12, 4385-4405,
32 doi:[10.5194/bg-12-4385-2015](https://doi.org/10.5194/bg-12-4385-2015), 2015.
- 33 Saito, K., Sueyoshi, T., Marchenko, S., Romanovsky, V., Otto-Bliesner, B., Walsh, J.,
34 Bigelow, N., Hendricks, A., and Yoshikawa, K.: LGM permafrost distribution:
35 how well can the latest PMIP multi-model ensembles perform reconstruction?,
36 *Climate of the Past*, 9, 1697-1714, doi:[10.5194/cp-9-1697-2013](https://doi.org/10.5194/cp-9-1697-2013), 2013.
- 37 Schuur, E. A., Bockheim, J., Canadell, J. G., Euskirchen, E., Field, C. B., Goryachkin, S.
38 V., Hagemann, S., Kuhry, P., Lafleur, P. M., and Lee, H.: Vulnerability of
39 permafrost carbon to climate change: Implications for the global carbon cycle,

- 1 BioScience, 58, 701-714, 2008.
- 2 Shi, Y., Mi, D., Feng, Q., Li, P., and Wang, Z.: Map of snow, ice and frozen ground in
3 China, China Cartographic Publishing House, Beijing, China, 1988.
- 4 Slater, A., and Lawrence, D.: Diagnosing Present and Future Permafrost from Climate
5 Models, Journal of Climate, 26, 5608–5623,
6 doi: <http://dx.doi.org/10.1175/JCLI-D-12-00341.1,2013>.
- 7 Swenson, S.C. and Lawrence, D.M.: A new fractional snow-covered area
8 parameterization for the Community Land Model and its effect on the surface
9 energy balance, J. Geophys. Res., 117, D21107, doi:10.1029/2012JD018178,
10 2012.
- 11 Tian, L., Li, W., Zhang, R., Tian, L., Zhu, Q., Peng, C., and Chen, H.: The Analysis of
12 Snow Information from 1979 to 2007 in Qinghai-Tibetan Plateau, Acta Ecologica
13 Sinica, 34 (20) : 5974-5983, 2014.
- 14 Van Duin, R. H. A.: The influence of management on the temperature wave near the
15 surface, Tech. Bull. 29, 21 pp., Inst. of Land and Water Manage. Res., Wageningen,
16 Netherlands, 1963.
- 17 Wang, C., and Shi, R.: Simulation of the land surface processes in the Western Tibetan
18 Plateau in summer, Journal of Glaciology and Geocryology, 29 (1), 73-81, 2007.
- 19 Wang, G., Li, Y., Wang, Y., and Wu, Q.: Effects of permafrost thawing on vegetation
20 and soil carbon pool losses on the Qinghai–Tibet Plateau, China, Geoderma, 143,
21 143-152, 2008.
- 22 Wang, K., Cheng, G., Jiang, C., and Niu, F.: Variation of Thermal Diffusivity and
23 Temperature Simulation of Soils of Vertical Heterogeneity in Nagqu Prefecture in
24 the Tibetan Plateau [J], Journal of Glaciology and Geocryology, 29 (3), 470-474,
25 2007.
- 26 Wang, T., Wang, N. L., and Li, S. X.: Map of the glaciers, frozen ground and desert in
27 China, 1: 4,000,000 (in Chinese) [J], Chinese Map Press, Beijing, China, 2006.
- 28 Wang, X., Yang, M., and Wan, G.: Processes of Soil Thawing-Freezing and Features of
29 Ground Temperature and Moisture at D105 on the Northern Tibetan Plateau,
30 Journal of Glaciology and Geocryology, 34, 56-63, 2012.
- 31 Wang, Z.: Applications of permafrost distribution models on the Qinghai-Tibetan
32 Plateau, Lanzhou University, 2010.
- 33 Wang, Z., Wang, X., and Li, Y.: Analyses of snow cover based on passive microwave
34 remote sensing data and observed data over the Tibetan Plateau [J], Journal of
35 Glaciology and Geocryology, 35(4), 783-792, 2013.
- 36 Wu, Q., and Liu, Y.: Ground temperature monitoring and its recent change in
37 Qinghai–Tibet Plateau, Cold Regions Science and Technology, 38, 85-92, 2004.

- 1 Wu, Q., and Niu, F.: Permafrost changes and engineering stability in Qinghai-Xizang
2 Plateau[J], Chinese Science Bulletin, 58(10): 1079-1094, 2013.
- 3 Wu, Q., and Zhang, T.: Changes in active layer thickness over the Qinghai - Tibetan
4 Plateau from 1995 to 2007, Journal of Geophysical Research: Atmospheres
5 (1984–2012), 115, D09107, doi:10.1029/2009JD012974, 2010.
- 6 Wu, T., Zhao, L., Li, R., Wang, Q., Xie, C., and Pang, Q.: Recent ground surface
7 warming and its effects on permafrost on the central Qinghai - Tibet Plateau[J],
8 International Journal of Climatology, 33(4): 920-930, 2013.
- 9 Wania, R., Ross, I., and Prentice, I.C.: Integrating peatlands and permafrost into a
10 dynamic global vegetation model: 2. Evaluation and sensitivity of vegetation and
11 carbon cycle processes, Global Biogeochem. Cycles, 23, GB3015,
12 doi:10.1029/2008GB003413, 2009.
- 13 Xin, Y., Wu, B., Bian, L., Liu, G., Zhang, L., and Li, R.: Simulation study of permafrost
14 hydro-thermo dynamics on Asian climate (in Chinese), the 29th annual meeting of
15 Chinese Meteorological Society, Shenyang, China, 2012-9-12, P461, 2012.
- 16 Xiong, J., Zhang, Y., Wang, S., SHang, L., CHen, Y., and SHen, X.: 1. Key Laboratory
17 of Land Surface Process and Climate Change in Cold and Arid Regions, Cold and
18 Arid Regions Environment Research Institute, Chinese Academy of Science,
19 Lanzhou 730000, China; 2. University of Chinese Academy of Sciences, Beijing
20 100049, China, PLATEAU METEOROLOGY, 33, 323-336, 2014.
- 21 Xu, X., and Lin, Z.: Remote sensing retrieval of surface monthly mean albedo in
22 Qinghai - Xizang Plateau, Plateau Meteorology, 21, 233-237, 2002.
- 23 Yao, T., Qin, D., Shen, Y., Zhao, L., Wang, N., and Lu, A.: Cryospheric changes and
24 their impacts on regional water cycle and ecological conditions in the Qinghai
25 Tibetan Plateau[J], Chinese J. Nature, 35: 179-186, 2013.
- 26 Yang, M., Nelson, F., Shiklomanov, N., Guo, D., and Wan, G.: Permafrost degradation
27 and its environmental effects on the Tibetan Plateau: A review of recent research,
28 Earth-Science Reviews, 103, 31-44, 2010.
- 29 Yang, M., Yao, T., Gou, X., Koike, T., and He, Y.: The soil moisture distribution,
30 thawing–freezing processes and their effects on the seasonal transition on the
31 Qinghai–Xizang (Tibetan) plateau, Journal of Asian Earth Sciences, 21, 457-465,
32 [http://dx.doi.org/10.1016/S1367-9120\(02\)00069-X](http://dx.doi.org/10.1016/S1367-9120(02)00069-X), 2003.
- 33 Yang, M., Yao, T., and Gou, X.: The freezing thawing processes and hydro-thermal
34 characteristics along the road on the Tbietan Plateau, Advancement of Natural
35 Science (China), 10 (5), 443-450, 2000.
- 36 Yang, M., Yao, T., and He, Y.: The extreme value analysis of the ground temperature
37 in northern part of Tibetan Plateau records from D110 site, Journal of Mountain
38 Science (China), 17 (3), 207-211, 1999.

- 1 Yu, F., Qi, J., Yao, X., and Liu, Y.: In-situ monitoring of settlement at different layers
2 under embankments in permafrost regions on the Qinghai–Tibet Plateau[J],
3 Engineering Geology, 160: 44-53, 2013.
- 4 Zhang, W., Wang, G., Zhou, J., Liu, G., and Wang, Y.: Simulating the Water-Heat
5 Processes in Permafrost Regions in the Tibetan Plateau Based on CoupModel,
6 Journal of Glaciology and Geocryology, 34, 1099-1109, 2012.
- 7 Zhang, Z., and Wu, Q.: Predicting changes of active layer thickness on the
8 Qinghai-Tibet Plateau as climate warming, Journal of Glaciology and
9 Geocryology, 34 (3), 505-511, 2012.
- 10 Zhou, Y., Guo, D., Qiu, G., Cheng, G., and Li, S.: China Permafrost, Science Press,
11 Beijing. p. 232. (inChinese), 2000.
- 12

1 Tables

2 Table 1. The six land surface models, analyzed over the Tibetan plateau (TP)

Model	Native Resolution	Number of soil layers	Depth of soil column (m)	Spatial domain	Atmospheric Forcing Data
CLM4.5 Swenson and Lawrence, 2012 Oleson et al., 2013	1 °×1.25 °	30	38.1	Whole TP	CRUNCEP4 ¹
CoLM Dai et al., 2003 Ji et al., 2014	1 °×1 °	10	2.86	Whole TP	Princeton ²
ISBA Decharme et al. 2011	0.5 °×0.5 °	14	10	Permafrost region follow IPA map	WATCH ³
JULES Best et al., 2011	0.5 °×0.5 °	30	2.95	Whole TP	WATCH ³
LPJ-GUESS Gerten et al., 2004 Wania et al., 2009	0.5 °×0.5 °	25	3	Permafrost region follow IPA map	CRU TS 3.1 ⁴
UVic Meissner et al., 2003	1.8 °×3.6 °	14	198.1	Whole TP	CRUNCEP4 ¹

3 ¹Viovy and Ciais (<http://dods.extra.cea.fr/>)

4 ²Sheffield et al. (2006) (<http://hydrology.princeton.edu/data.pgf.php>)

5 ³Weedon et al. (2011) (<http://www.waterandclimatechange.eu/about/watch-forcing-data-20th-century>)

6 ⁴Harris et al. (2013), University of East Anglia Climate Research Unit (2013)

7

- 1 Table 2. The five diagnostic methods and threshold values used to derive permafrost.
- 2 The thresholds commonly used in the literature and in this paper are marked in bold.

Method	Definition	Threshold	Data used for calculation
TSL	More than 24 consecutive months soil temperature \leq a threshold	0 °C	0 ~ 3m monthly soil temperature
MAGT	Mean annual of 3 m soil temperature \leq a threshold	0 °C, 0.5 °C	Mean annual of 3 m soil temperature
SFI	Surface frost number \geq a threshold	0.4, 0.5 , 0.6	Annually maximum and minimum ground surface temperature
F	Air frost number \geq a threshold	0.4, 0.5 , 0.6	Annually maximum and minimum air temperature
MAAT	Mean annual air temperature \leq a threshold	0 °C, -1 °C, -2 °C, -3 °C	Mean annual of air temperature

3

4

1 Table 3. Derived permafrost area inside the common modeling region on Tibetan
 2 plateau (10^4 km^2) from 6 LSMs and 5 diagnostic methods, using different thresholds.
 3 The results of thresholds commonly used in the literature and in this paper are marked
 4 in bold.

		CLM4.5	CoLM	JULES	UVic	ISBA	LPJ-GUESS	across-model uncertainty
Indirect method	MAAT ≤ 0 °C	130	124	126	116	127	129	14
	MAAT ≤ -1 °C	122	117	119	109	119	120	13
	MAAT≤ -2 °C	113	105	111	99	109	110	14
	MAAT ≤ -3 °C	95	83	96	81	91	93	15
	across-threshold uncertainty	35	41	30	35	36	36	
	F ≥ 0.4	140	135	138	126	138	138	14
	F≥ 0.5	135	127	131	118	130	131	17
	F ≥ 0.6	117	93	106	89	100	101	28
	across-threshold uncertainty	23	42	32	37	38	37	
Direct method	TSL	60	1	62	8	44	119	118
	MAGT ≤ 0.5 °C	112	102	104	8	72	131	123
	MAGT≤ 0 °C	104	89	96	8	61	128	120
	across-threshold uncertainty	8	13	8	0	11	3	
	SFI ≥ 0.4	135	122	130	32	131	127	103
	SFI≥ 0.5	116	62	100	8	113	119	111
	SFI ≥ 0.6	42	17	38	4	55	104	100
	across-threshold uncertainty	93	105	92	28	76	23	
across-direct method uncertainty (based on commonly used methods TSL, MAGT≤ 0°C, SFI≥ 0.5)	56	88	38	0	69	9		

5

1 Table 4. Model - observed temperatures differences in mean annual and seasonal cycle
 2 amplitude of air and soil temperature, based on data from 1996-2000 (section 3.4;
 3 Figure 4), and the corresponding vegetation and soil properties of both observation and
 4 models. Air temperature data is only available for D66 station and limited from 1997/9
 5 to 1998/8. Thus the statistics of ground temperature of D66 is also confined to this
 6 period .

D66 (35.63 N, 93.81 E)									
	Temperature bias "Model - Observation"						Soil conditions		
	Air temperature		Ground temperature				Bare ground	Vegetation	Texture (top soil)
	Mean annual	Seasonal amplitude	At 0.04 m depth		At 2.63 m depth				
			Mean annual	Seasonal amplitude	Mean annual	Seasonal amplitude			
Obs ¹							100%	None	gravel
CLM4.5 ²	4.3	1	2	-0.2	2	3.5	81%	10% boreal shrub 8% C3 arctic grass	63% sand 19% clay
CoLM ³	2.3	0.1	0	0.1	-1	2.4	87%	4% boreal shrub 5% C3 arctic grass 3% C3 non arctic grass	43% sand 18% clay
ISBA ⁴	1.4	0.1	-1.3	-1.3	0.8	0.5	53%	46% C3 grass	55% sand 7% clay
JULES [#]	1.1	0.3	-0.5	2.1	-2	4			
LPJ-GUESS ^{*5}	1.5	-0.1	-3.4	-6.6	-3.7	1.5		tundra	clay-like
UVic ⁶	2.6	0.5	7.5	-1.5	7.6	2.1	100%	None	44% sand 24% clay

7

8

1

D105 (33.07 N, 91.94 E)					
	Temperature bias "Model - Observation"		Soil conditions		
	Ground temperature				
	At 3 m depth		Bare ground	Vegetation	Texture (top soil)
	Mean annual	Seasonal amplitude			
Obs ⁷			50%-60%	grass (<i>Leontopodium nanum</i>)	coarse and fine sand
CLM4.5 ²	-1.2	0.8	48%	17% boreal_shrub 30% C3 arctic grass	60% sand 20% clay
CoLM ³	0.1	0.2	7%	69% C3 arctic grass 24% C3 non arctic grass	38% sand 16% clay
ISBA ⁴	0.9	-0.9	27%	72% C3 grass	52% sand 10% clay
JULES [#]	-1.8	1.8			
LPJ -GUESS ^{*5}	-3.7	0.7		tundra	clay-like
UVic ⁶	1	-0.2	7%	33% C3 grass 60% shrub	43% sand 32% clay

2

3

4

1

D110 (32.82 N, 93.01 E)					
	Temperature bias "Model - Observation"		Soil conditions		
	Ground temperature				
	At 0.04 m depth		Bare ground	Vegetation	Texture (top soil)
	Mean annual	Seasonal amplitude			
Obs ⁸			60-70%	grass (<i>Kobresia humilis</i>)	coarse and fine sand
CLM4.5 ²	-1.8	1	33%	7% boreal_shrub 57% C3 arctic grass	60% sand 21% clay
CoLM ³	0.5	1.4	1%	56% C3 arctic grass 43% C3 non arctic grass	45% sand 17% clay
ISBA ⁴	-1.4	0.8	10%	89% C3 grass	50% sand 11% clay
JULES [#]	-1.9	0.9			
LPJ-GUESS ^{*5}	-4.1	-3.7		tundra	clay-like
UVic ⁶	1.1	-0.5	6%	31% C3 grass 60% shrub	45% sand 30% clay

2

3 ¹Yang et al. (2000)

4 ²https://dl.dropboxusercontent.com/u/41730762/surfdata_0.9x1.25_simyr1850_c130415.nc

5 ³Dai et al. (2003); Ji et al. (2014)

6 ⁴Harmonized World Soil Database

7 ⁵Thermal diffusivities follow Van Duin (1963) and Jury et al. (1991), volumetric fraction of organic
8 material follow Hillel (1998), water held below wilting point and porosity from AWFA (2002)

9 ⁶Scholes and de Colstoun (2012) (<http://www.daac.ornl.gov>)

10 ⁷Wang et al. (2012)

11 ⁸Yang et al. (1999)

12 * The classification of soil texture is based on soil volumetric water holding capacity, thermal
13 diffusivities, volumetric fraction of organic material, water held below wilting point and porosity

14 #This model doesn't provide soil parameter information

15

16

17

1 Table 5. Description of Model Characteristics Relevant to Soil Temperatures on TP

Model	Snow cover ¹	Albedo ²	Soil water ³	Unfrozen water effect during phase change ⁴	Surface Organic layer insulation	Snow scheme ⁵
CLM4.5	Medium	Medium	Medium	Yes	Yes	Dynamic & ML
CoLM	Medium	Medium	Medium	No	No	Dynamic & ML
ISBA	Low	Low	Medium	Yes	Yes	Static & ML
JULES	Low	Low	Medium	Yes	No	Dynamic & ML
LPJ-GUESS	Medium	Low	High	No	No	Static & BL
UVic	None	Low	High	Yes	No	Static & I

2 ¹ Low snow cover is confined to high elevations, medium tends to be on western TP

3 ² LPJ-GUESS has constant albedo everywhere and UVic albedo varies slightly due to
 4 vegetation, year-round albedo variability for other models depends mainly on snow
 5 cover in winter and soil moisture, vegetation, etc in summer

6 ³ soil water content includes both liquid and ice fractions

7 ⁴ all models calculate soil thermal properties depending on soil moisture and also phase
 8 change of water, but CoLM and LPJ-GUESS ignore solute dependent freezing
 9 processes

10 ⁵ Dynamic or static snow layering; ML: Multi-layer, BL: Bulk-layer, I: Implicit;
 11 according to *Slater et al.* [2001]

12

13

1 Table 6. Derived permafrost area (10^4 km^2) with deeper soil layers using the TSL
2 method. The results for thresholds commonly used in the literature and in this paper are
3 marked in bold.

4

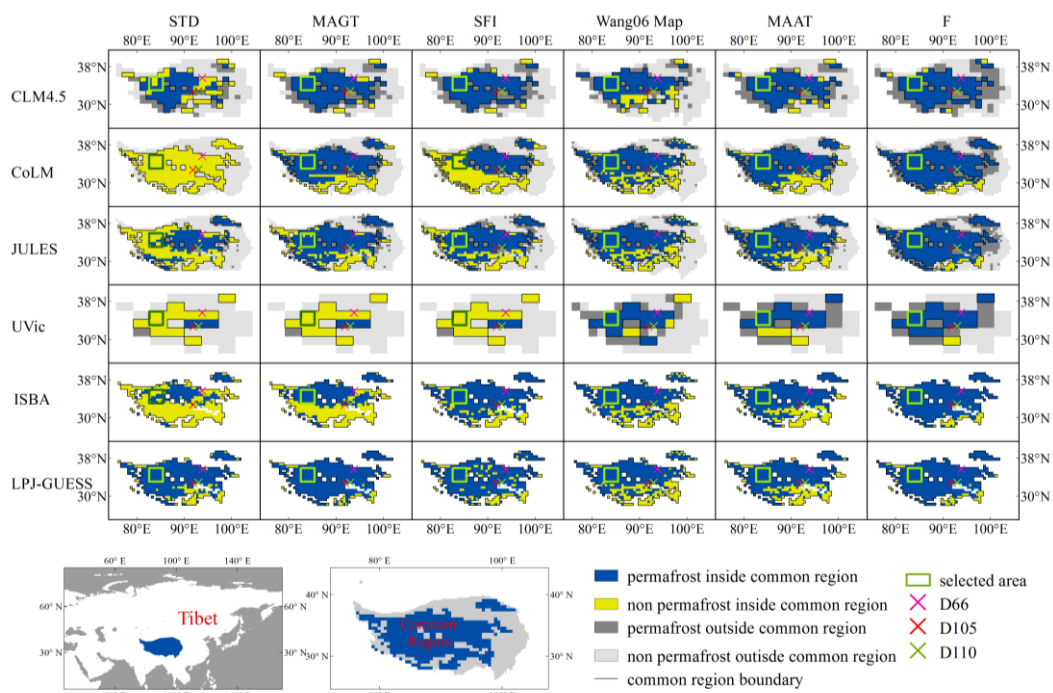
Depth of deepest layer used for calculation	CLM4.5	ISBA
3 m	60	44
5 m	85	54

5

6

7

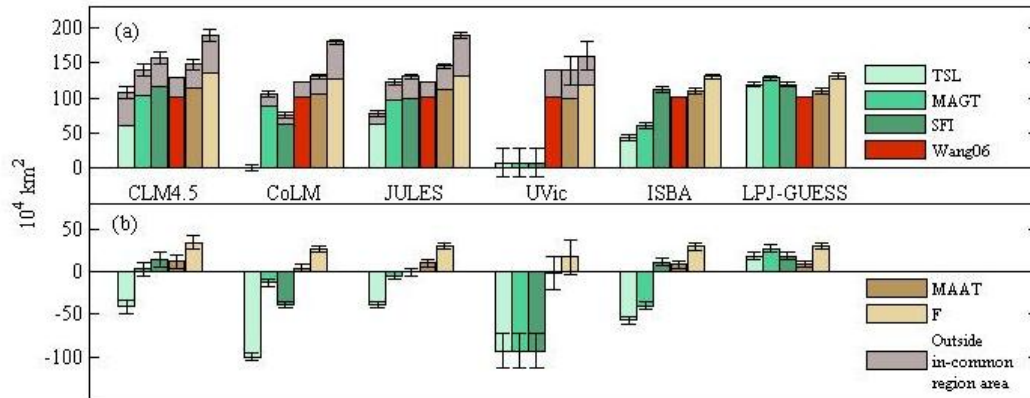
1 Figure Captions



2

3 **Figure 1.** Permafrost maps derived from different diagnostic methods and models
 4 compared with Wang06 map. Permafrost inside the common modeling region is used
 5 for all-models inter-comparison, while permafrost outside allows further evaluation
 6 over the whole TP for CLM4.5, CoLM, JULES and UVic. The observation-based map
 7 of permafrost (Wang et al., 2006) is re-gridded to match model resolution. The selected
 8 area in the western TP (33 °- 36 °N, 82.5 °- 85.5 °E) is used to examine across-model
 9 differences in Figure 5. Insets show location map of TP and how the common region is
 10 related to the TP.

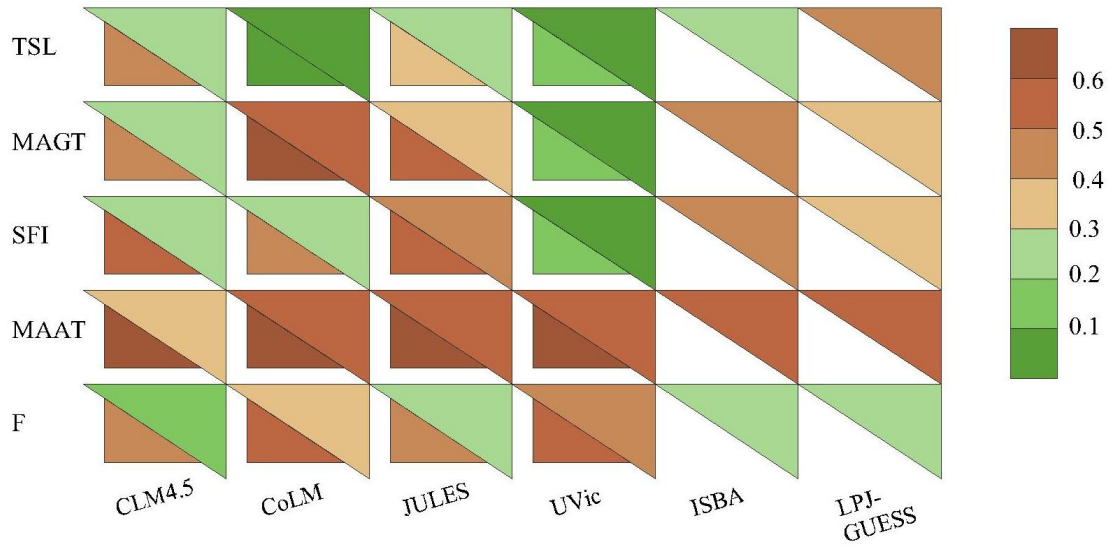
11



1

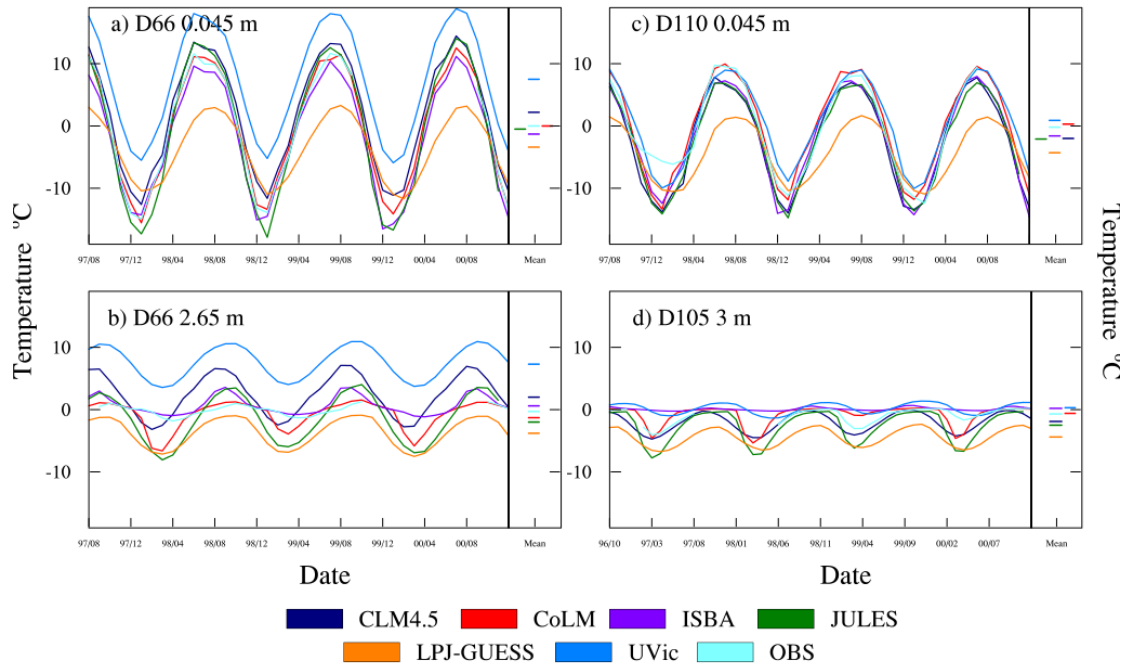
2 **Figure 2.** Permafrost areas derived from different diagnostic methods compared with
 3 Wang06 map. (a) Permafrost area, with TP permafrost outside the common region
 4 denoted by grey extensions to the bars for CLM4.5, CoLM, JULES and UVic. (b) Bias
 5 in permafrost area “Model minus Wang06 estimate”, only for the common modeling
 6 region. The error bar is calculated as half of the averaged grid cell area of the model, so
 7 is model resolution dependent.

8



1
2
3
4
5
6

Figure 3. Kappa coefficient, K , quantifying the agreement between model-derived and Wang06 maps (see section 3.3). $K \geq 0.2$ indicates at least fair agreement with Wang06 map. The lower triangle is K for the whole TP and is only available for CLM4.5, CoLM, JULES and UVic, while the upper triangle is K for the common modeling region.

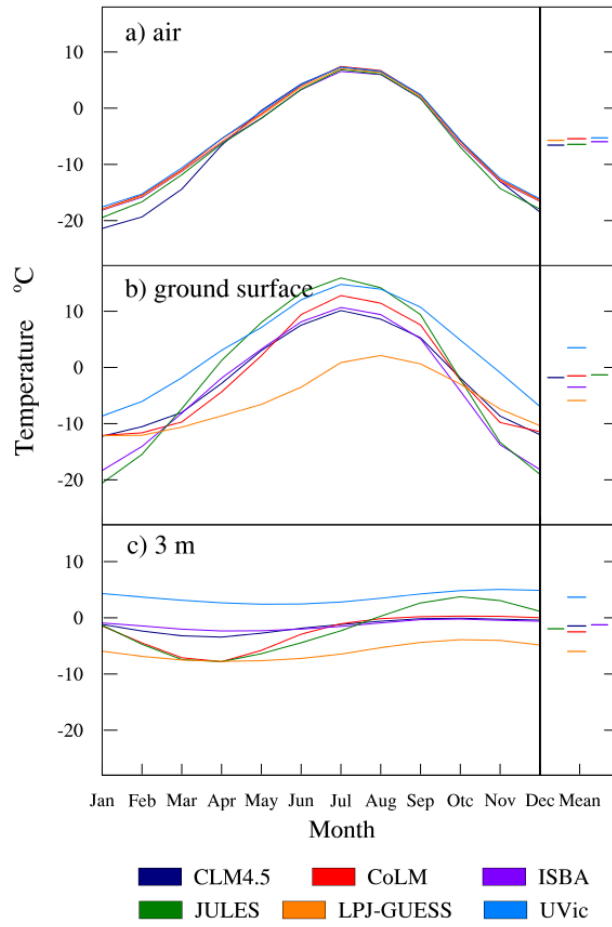


1

2 **Figure 4.** Monthly soil temperature variations at 3 stations from models and
 3 observations. (a) and (c) soil temperature of top layer. (b) and (d) soil temperature of
 4 deeper layer, 1996-2000. “Mean” denotes annual average temperature. We use the
 5 topmost available soil temperatures (0.04 m at D66 and D110, no good data for D105)
 6 and lowest available ones (2.63 m at D66, 3 m of D105), while D110 has only
 7 temperatures at 2 m depth.

8

9

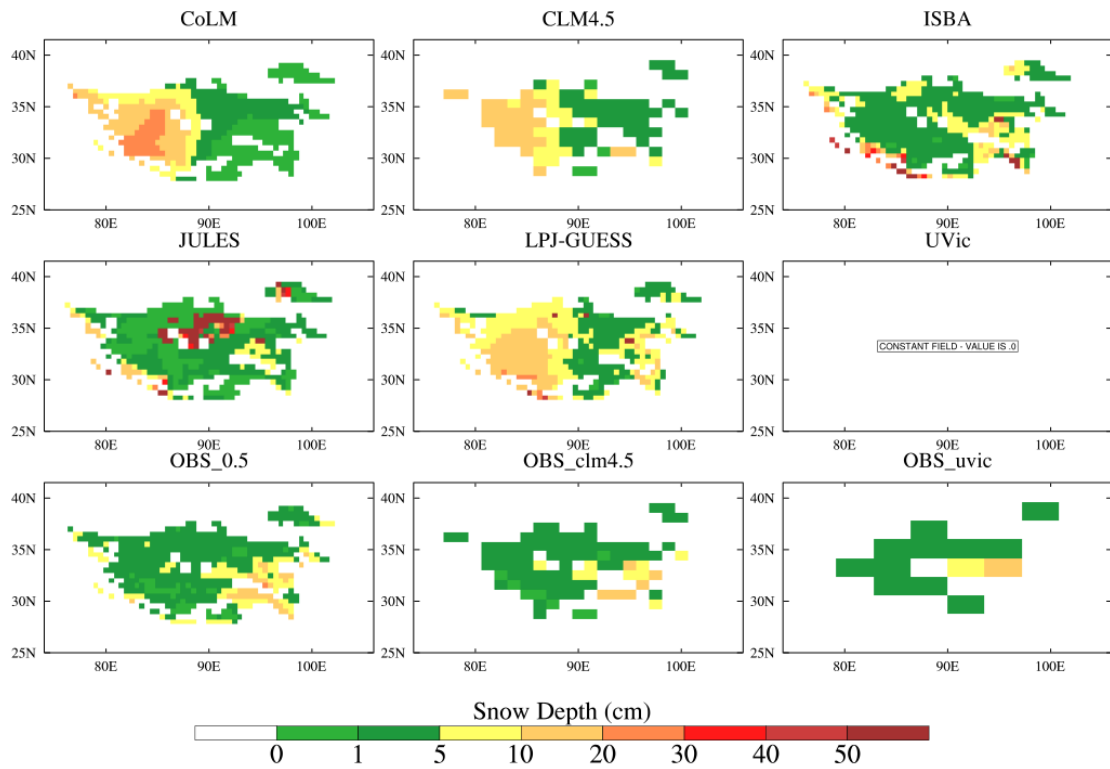


1

2 **Figure 5.** Monthly temperatures averaged over the selected western TP area in Figure 1.

3 (a) Forcing air temperature, (b) Ground surface temperature, (c) 3 m soil temperature,

4 averaged over 1980-2000. “Mean” denotes annual average temperature.

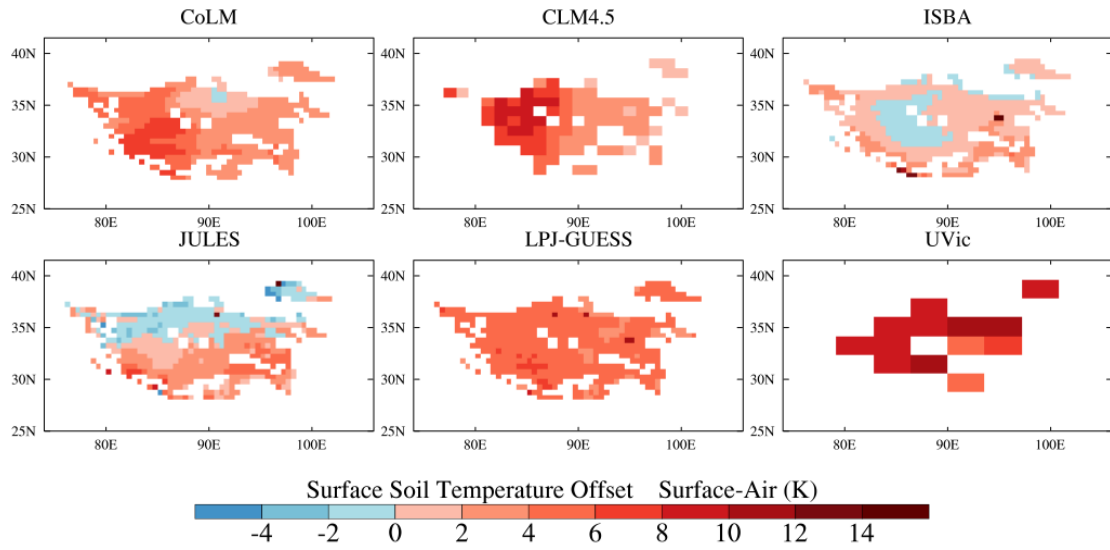


1

2 **Figure 6.** Winter snow depth for the common region, averaged over 1980-2000. Note
 3 the nonlinear color scale. We use the Long Time Series Snow Dataset of China (Che et
 4 al., 2008) (<http://westdc.westgis.ac.cn>) as observed snow depth. The observed snow
 5 depth plot is further interpolated onto the models' resolutions as "OBS_". The OBS_05
 6 is in 0.5 °resolution for CoLM, ISBA, JULES and LPJ-GUESS. The OBS_CLM4.5 and
 7 OBS_UVic are in the resolutions of CLM4.5 and UVic separately.

8

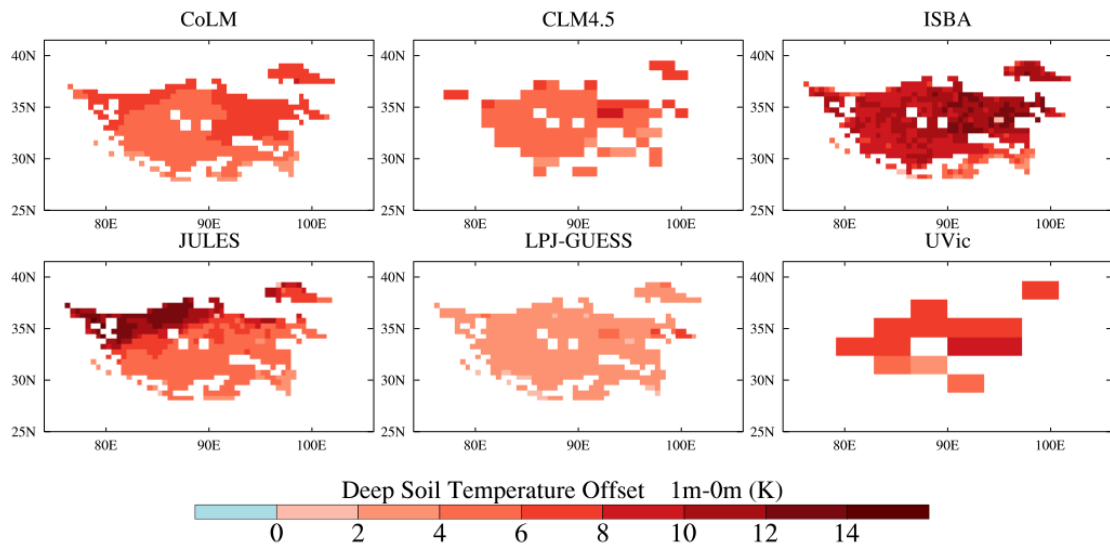
9



1

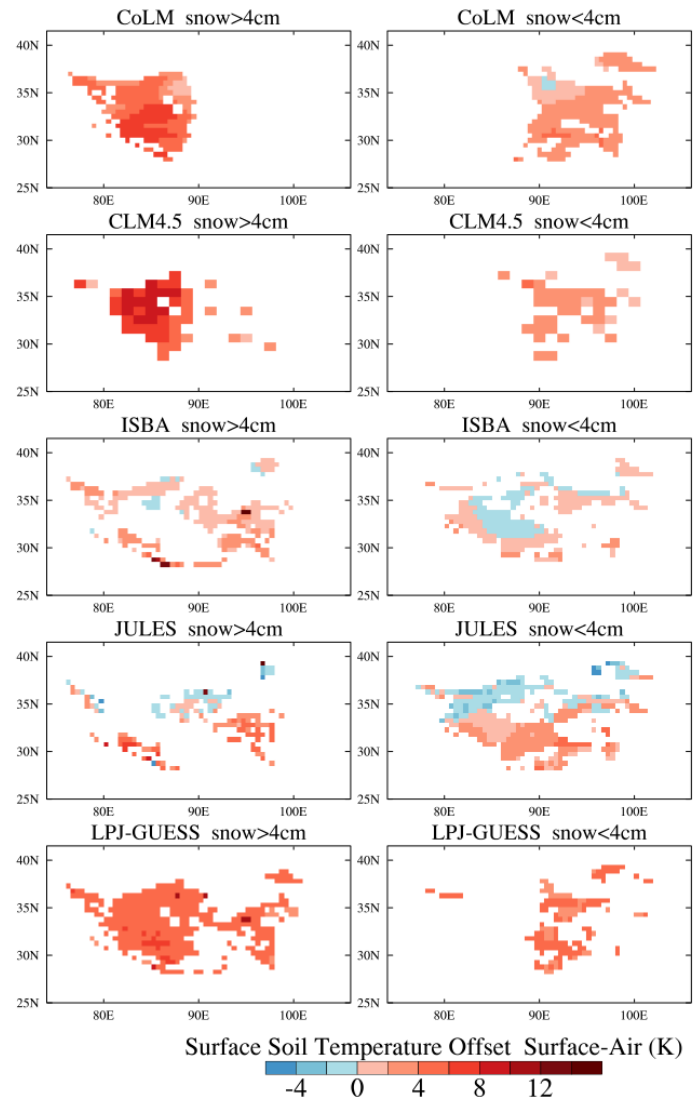
2 **Figure 7.** Mean surface temperature offset: difference in mean winter temperatures
 3 between surface soil and air, averaged over 1980-2000. Warm colors indicate soil is
 4 warmer than air temperature.

5

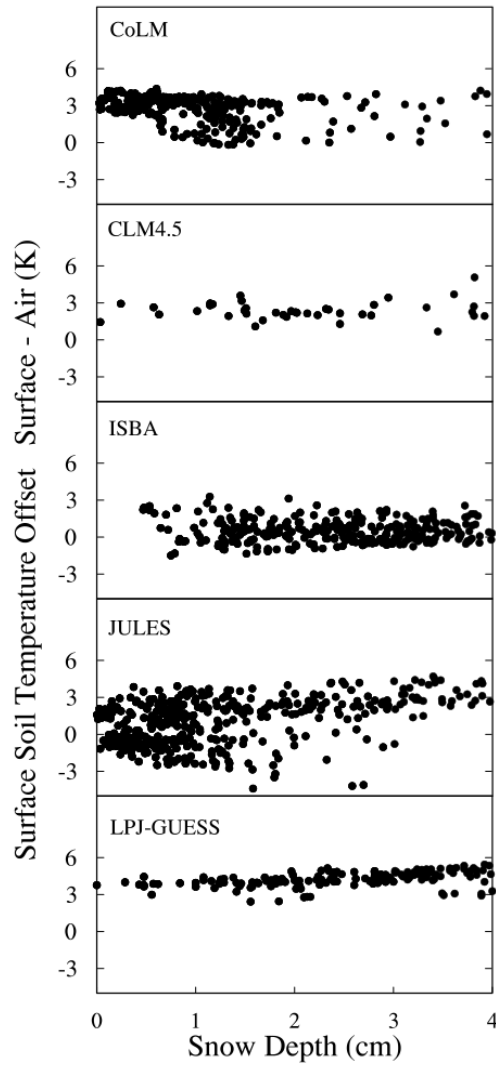


1

2 **Figure 8.** Mean soil temperature offset: difference in mean winter temperatures
 3 between soil at 1 m depth and surface soil, averaged over 1980-2000. Warm colors
 4 indicate deep soil is warmer than shallow soil.



1
 2 **Figure 9.** Mean surface temperature offset (difference in mean winter temperatures
 3 between surface soil and air, averaged over 1980-2000). Left column is for snow
 4 depth > 4 cm, right column shows regions with snow depth < 4 cm. Warm colors
 5 indicate soil is warmer than air temperature.



1

2 **Figure 10.** Mean surface temperature offset (difference in mean winter temperatures
 3 between surface soil and air, averaged over 1980-2000) as a function of snow depth for
 4 grid points where average snow depth < 4 cm.

5